 CMES, vol.40, no.3, pp.271-305, 2009

Micromechanical analysis of aligned and randomly oriented whisker-/ short fiber-reinforced composites

S.H. Pyo[1] **and H.K. Lee**[1,2]

Abstract: This paper presents a micromechanical approach for predicting the elastic and multi-level damage response of aligned and randomly oriented whisker-/ short fiber-reinforced composites. Based on a combination of Eshelby's micromechanics and the evolutionary imperfect interface approach, the effective elastic moduli of the composites are derived explicitly. The modified Eshelby's tensor for spheroidal inclusions with slightly weakened interface [Qu (1993b)] is extended in the present study to model whiskers or short fibers having mild or severe imperfect interfaces. Aligned and random orientations of spheroidal reinforcements are considered. A multi-level damage model in accordance with the Weibull's probabilistic function is then incorporated into the micromechanical framework to describe the sequential, progressive imperfect interfaces in the composites. Numerical examples corresponding to uniaxial tensile loadings are solved to illustrate the potential of the proposed micromechanical framework for predicting the elastic and multi-level damage response of the composites. Furthermore, comparisons between the present predictions and experimental data in the literature are made to further highlight the capability of the proposed micromechanical framework.

Keywords: Multi-level damage modeling, Modified Eshelby's tensor, Progressive imperfect interface, Spheroidal reinforcements, Aligned and random orientations.

1 Introduction

Nowadays, there have been growing interests in whisker- or short fiber-reinforced composites in various engineering application such as automotive, electronics and construction fields because of their ease of fabrication, economy and superior mechanical/electrical properties [Huang (2001); Nguyen and Khaleel (2004); Maity,

[1] Department of Civil and Environmental Engineering, Korea Advanced Institute of Science and Technology, Daejeon 305-701, South Korea
[2] Corresponding author: leeh@kaist.ac.kr

Jacob, Das, Alam, and Singh (2008)]. In general, fibers (e.g., glass, carbon, SiC, TiB, dispersed carbon nanotube, etc.) are embedded in the form of whiskers or short fibers in the matrix. Those composites have more balanced properties, which leads to an improved through-the-thickness stiffness/strength and a better ability to formulate complex shapes [Huang (2001)]. Several methodologies were made in order to predict mechanical behavior of composite materials [e.g., Takashima, Nakagaki, and Miyazaki (2007); Pahr and Böhm (2008)]. However, it is difficult to predict the overall behavior of those composites numerically or experimentally due to the complexity of their microstructure and damage mechanisms (e.g., fiber/matrix debonding, matrix microcracking) [Nguyen and Khaleel (2004)]. That is, one could say that the condition of perfect bonding at the interface between inclusions and the matrix is often inappropriate in addressing the physical nature and mechanical behavior of the interface [Gao (1995)]. Therefore, several approaches have been proposed for evaluating the effective elastic properties of composites with these discontinuous reinforcements considering various damage phenomena [e.g., Joseph, Thomas, and Pavithran (1996); Tucker III and Liang (1999); Hine, Rudolf Lusti, and Gusev (2002); Arbelaiz, Fernández, Ramos, Retegi, Llano-Ponte, and Mondragon (2005); Chen and Ke (2008); Oyekoya, Mba, and El-Zafrany (2008)].

Micromechanics, which encompasses mechanics related to the microstructure of materials, can be applied to study and elucidate the influence of defects such as microcracks, flaws, pores, and inclusions, including impurities and precipitates, on the elastic and mechanical behavior of materials [Mura (1982); Nemat-Nasser and Hori (1993); Luo and Stevens (1996)]. An elastoplastic model for two-phase metal matrix composites containing randomly located yet aligned spheroidal inclusions based on ensemble-volume averaging procedure was proposed by Ju and Sun (2001) and Sun and Ju (2001). Micromechanical damage constitutive models for aligned and randomly oriented discontinuous fiber reinforced composites are presented by Lee and Simunovic (2000, 2001). Sun, Ju, and Liu (2003) proposed an elastoplastic damage model for spheroidal inclusions reinforced composites considering partial debonding of inclusions. Recently, elastic and elastoplastic damage models for spherical and cylindrical inclusions reinforced composites considering multi-level damage process based on the Eshelby's micromechanics were proposed in our preceding works [Lee and Pyo (2007, 2008a, 2008b, 2009); Pyo and Lee (2009a, 2009b)].

The primary objective of the present study is to develop a three-dimensional (3D) micromechanics based progressive damage model to predict the effective elastic moduli and damage evolution in aligned and randomly oriented whisker- and short fiber-reinforced composites. Short fibers (or whiskers) embedded in the composites are modeled as spheroidal reinforcements in the present study. Moreover, the Es-

helby's tensor for an ellipsoidal inclusion with slightly weakened interface derived by Qu (1993a, b) is extended in order to model spheroidal reinforcements having imperfect interfaces in the composites. Fibers (or whiskers) are assumed to be non-interacting, randomly dispersed yet aligned or randomly oriented and initially embedded firmly in the matrix with perfect bonded interfaces. It is also assumed that the progression of imperfect interface is governed by multi-level damage process based on Weibull's statistical function [Lee and Pyo (2008a)] where the average internal stresses of perfectly bonded fibers (phase 1) and the Weibull parameters are the controlling factors.

Following the multi-level damage process proposed in our preceding work [Lee and Pyo (2008a)], a three-level elastic damage model is adopted for a complete description of the sequential progression of imperfect interface in the composites, which is illustrated in Figure 1. As seen in Figure 2, aligned and random orientations of spheroidal reinforcements are considered in accordance with Lee and Simunovic (2000), Sun and Ju (2004), and Qiu and Weng (1990). In order to illustrate the potential of the proposed micromechanical framework, numerical examples of the composites under uniaxial tension are presented. Parametric studies of model parameters are conducted to clearly address the influence of the parameters on the progression of imperfect interface in the composites. Finally, the applicability of the proposed micromechanical framework is highlighted by comparing the present predictions with available experimental data in the literature.

The present paper is organized as follows. Effective elastic moduli of composites containing randomly located and aligned spheroidal reinforcements is micromechanically constructed in Section 2. Effective elastic moduli of composites containing randomly oriented reinforcements are explicitly derived based on the orientational averaging approaches proposed by Lee and Simunovic (2000), Sun and Ju (2004), and Qiu and Weng (1990) in Section 3. In Section 4, a multi-level damage model [Lee and Pyo (2008a)] for progressive imperfect interface in accordance with the Weibull's probabilistic function is recapitulated and internal stresses of reinforcements are formulated. A series of parametric analysis to address the influence of model parameters on the progressive imperfect interface in the composites with aligned and 3D randomly oriented reinforcements are conducted in the Sections 5 and 6, respectively. Finally, the present prediction are compared with experimental data [Fu, Lauke, Mäder, Yue, and Hu (2000); Gorsse and Micracle (2003)] to highlight the capability of the proposed micromechanical framework in Section 7.

2 Effective elastic moduli of composites containing aligned spheroidal reinforcements

Let us consider an initially perfectly bonded two-phase composite consisting of an elastic matrix (phase 0) with bulk modulus κ_0 and shear modulus μ_0, and randomly located yet aligned elastic spheroidal reinforcements (phase 1) with bulk modulus κ_1 and shear modulus μ_1. All reinforcements are assumed to be non-interacting and initially embedded firmly in the matrix with perfect interfaces.

As external loads or deformations continue to increase, some initially perfectly bonded reinforcements are transformed statistically to reinforcements with mild imperfect interface (phase 2). Some reinforcements with mild imperfect interface are then transformed to reinforcements with severe imperfect interface (phase 3). Finally, all reinforcements are transformed to completely debonded reinforcements that are regarded as spheroidal voids (phase 4). The schematic of this multi-level damage transition is shown in Figure 1.

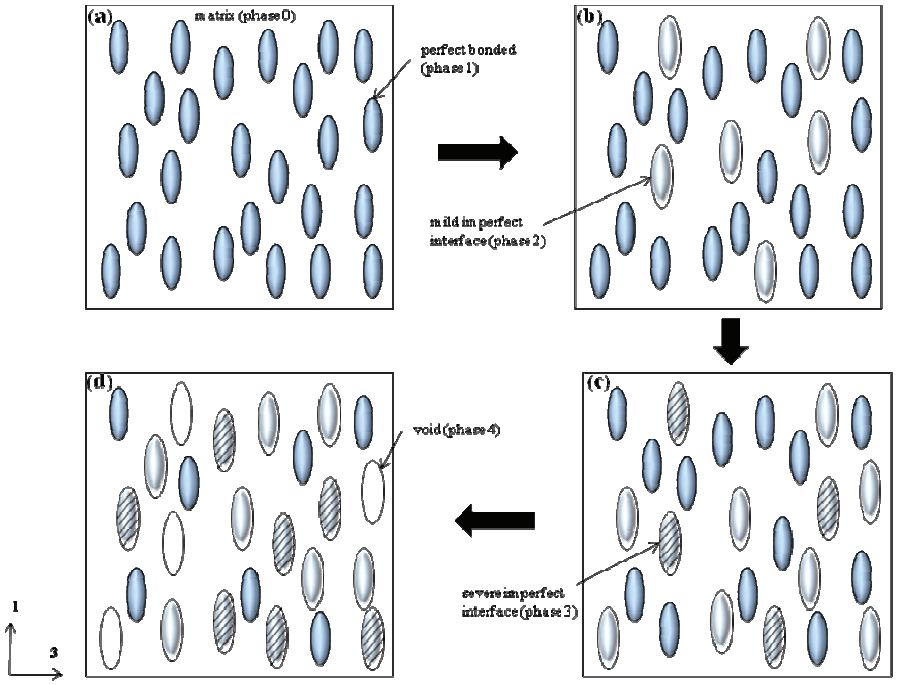

Figure 1: Schematics of multi-level damage evolution in a composite with: (a) two-phase composite state (initial state); (b) three-phase composite state; (c) four-phase composite state; (d) five-phase composite state (cf. Lee and Pyo, 2008a)

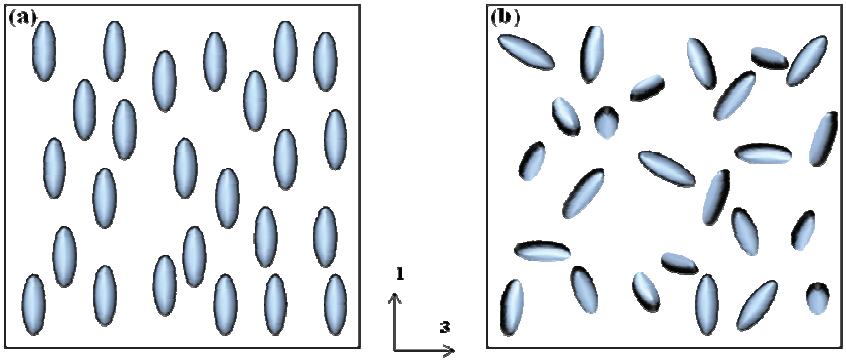

Figure 2: Schematics of aligned (a) and 3D randomly oriented (b) spheroidal reinforcements

The effective stiffness tensor $\mathbf{C}^*$ for multi-phase, linear elastic composites containing arbitrarily non-aligned and/or dissimilar inclusions can be derived as [Ju and Chen (1994)]

$$\mathbf{C}^* = \mathbf{C}_0 \cdot \left\{ \mathbf{I} + \sum_{r=1}^{4} \left[\phi_r (\mathbf{A}_r + \mathbf{S}_r)^{-1} \cdot \{ \mathbf{I} - \phi_r \mathbf{S}_r \cdot (\mathbf{A}_r + \mathbf{S}_r)^{-1} \}^{-1} \right] \right\} \tag{1}$$

where "" is the tensor multiplication, $\mathbf{C}_r$ is the elasticity tensor of the r-phase, $\mathbf{I}$ is the fourth-rank identity tensor, ϕ_r denotes the volume fraction of the r-phase inclusion, $\mathbf{S}_r$ denotes Eshelby's tensor of the r-phase, and the fourth-rank tensor $\mathbf{A}_r$ is defined as $\mathbf{A}_r \equiv (\mathbf{C}_r - \mathbf{C}_0)^{-1} \cdot \mathbf{C}_0$.

The interior-point Eshelby's tensors $\mathbf{S}_1$ for perfectly bonded spheroidal reinforcements and $\mathbf{S}_4$ for completely debonded spheroidal reinforcements (voids) were explicitly given by Ju and Sun (1999) as

$$(S_{1,4})_{ijkl} = \frac{1}{4(1-\nu_0)} \left[S^{(1)}_{IK} \delta_{ij} \delta_{kl} + S^{(2)}_{IJ} (\delta_{ik} \delta_{jl} + \delta_{il} \delta_{jk}) \right] \tag{2}$$

where ν_0 denotes the Poisson's ratio of the matrix and δ_{ij} signifies the Kronecker delta. The components of the second-rank tensors $S^{(1)}_{IK}$ and $S^{(2)}_{IJ}$ can be found in Ju and Sun (1999).

The Eshelby's tensor for an ellipsoidal inclusion with slightly weakened interface proposed by Qu (1993a, b) can be written as

$$S^M_{ijkl} = \frac{1}{\Omega} \int_\Omega S^O_{ijkl}(\mathbf{x}) dV(\mathbf{x}) = S^O_{ijkl} + (I_{ijpq} - S^O_{ijpq}) H_{pqrs} L_{rsmn} (I_{mnkl} - S^O_{mnkl}) \tag{3}$$

where Ω denotes an ellipsoidal subdomain in a homogeneous and linearly elastic solid, $\mathbf{L}$ signifies the fourth-rank elasticity tensor, S^O_{ijkl} is the original Eshelby's tensor and the fourth-rank tensor $\mathbf{H}$ is given by Qu (1993a, b)

$$H_{ijkl} = \frac{1}{4\Omega}\int_s (\eta_{ik}n_j n_l + \eta_{jk}n_i n_l + \eta_{il}n_j n_k + \eta_{jl}n_i n_k)dS \tag{4}$$

In the case of ellipsoidal inclusions, H_{ijkl} can be expressed as [Qu (1993b)]

$$H_{ijkl} = \alpha P_{ijkl} + (\beta - \alpha)Q_{ijkl} \tag{5}$$

in which

$$P_{ijkl} = \frac{3}{16\pi}\int_0^{\pi}\left[\int_0^{2\pi}(\delta_{ik}\hat{n}_j\hat{n}_l + \delta_{jk}\hat{n}_i\hat{n}_l + \delta_{il}\hat{n}_k\hat{n}_j + \delta_{jl}\hat{n}_k\hat{n}_i)n^{-1}d\theta\right]\sin\phi\, d\phi \tag{6}$$

$$Q_{ijkl} = \frac{3}{4\pi}\int_0^{\pi}\left[\int_0^{2\pi}\hat{n}_i\hat{n}_j\hat{n}_k\hat{n}_l n^{-3}d\theta\right]\sin\phi\, d\phi \tag{7}$$

where unit normal vector $\mathbf{n}$ can be defined as [Qu (1993b)]

$$\hat{\mathbf{n}} = \left(\frac{\sin\phi\cos\theta}{a_1}, \frac{\sin\phi\sin\theta}{a_2}, \frac{\cos\phi}{a_3}\right)^T \tag{8}$$

with

$$n = \sqrt{\hat{n}_i\hat{n}_i} \tag{9}$$

in which a_i denotes the radius of the inclusions, and α and β represent the compliances in the tangential and normal directions of the interface [Qu (1993a, b)]. Further details of the Eshelby's tensor for an ellipsoidal inclusion with slightly weakened interfaces can be found in Qu (1993a, b).

By carrying out the lengthy algebra but straightforward, the Eshelby's tensor for a spheroidal inclusion ($a_1 \neq a_2 = a_3$) with imperfect interface embedded in an isotropic linear elastic and infinite matrix are (newly) derived based on Qu (1993a, b)'s modified Eshelby's tensor in Eq. (3) as follows:

$$(S_{n+1})_{ijkl} = \frac{1}{4(1-\nu_0)}\left[S^{M(2n-1)}_{IK}\delta_{ij}\delta_{kl} + S^{M(2n)}_{IJ}(\delta_{ik}\delta_{jl} + \delta_{il}\delta_{jk})\right] \tag{10}$$

where n = 1, 2 (1 and 2 indicate the mild and severe imperfect interface stages, respectively). In addition, the components of the second-rank tensors $S^{M(2n-1)}_{IK}$ and $S^{M(2n)}_{IJ}$ read

$$S_{11}^{M(2n-1)} = S_{11}^{(1)} + \frac{1}{12a[1-\nu_0][\gamma^2-1]^2}$$
$$\left[\begin{array}{c} 9\varsigma_{10}(\gamma)\{(\beta_n-\alpha_n)(\zeta_1(\gamma)\varsigma_1(\gamma)-2\zeta_3(\gamma)\varsigma_9(\gamma))+\alpha_n\zeta_4(\gamma)\varsigma_1(\gamma) \\ -8\alpha_n\zeta_5(\gamma)\varsigma_3(\gamma)\{1+3\varsigma_2(\gamma)\} \\ +\{2\varsigma_3(\gamma)-4\mu_0(1+3\varsigma_2(\gamma))\}\left\{\begin{array}{c} 3(\beta_n-\alpha_n)(2\zeta_2(\gamma)\varsigma_9(\gamma)-\zeta_3(\gamma)\varsigma_1(\gamma) \\ +2\alpha_n\zeta_5(\gamma)\varsigma_4(\gamma) \end{array}\right\} \end{array}\right] \tag{11}$$

$$S_{12}^{M(2n-1)} = S_{13}^{M(2n-1)} = S_{12}^{(1)} + \frac{1}{16a[1-\nu_0][\gamma^2-1]^2}$$
$$\left[\begin{array}{c} 3\{\mu_0\varsigma_5(\gamma)+\varsigma_6(\gamma)\}\{(\beta_n-\alpha_n)(2\zeta_3(\gamma)\varsigma_9(\gamma)-\zeta_1(\gamma)\varsigma_1(\gamma))-\alpha_n\zeta_4(\gamma)\varsigma_1(\gamma)\} \\ -16\alpha_n\zeta_5(\gamma)\varsigma_{12}(\gamma)\{1+3\varsigma_2(\gamma)\} \\ +4\varsigma_{12}(\gamma)\{3(\beta_n-\alpha_n)(2\zeta_2(\gamma)\varsigma_9(\gamma)-\zeta_3(\gamma)\varsigma_1(\gamma))+2\alpha_n\zeta_5(\gamma)\varsigma_4(\gamma) \end{array}\right] \tag{12}$$

$$S_{21}^{M(2n-1)} = S_{31}^{M(2n-1)} = S_{21}^{(1)} + \frac{3}{8a[1-\nu_0][\gamma^2-1]^2}$$
$$\left[\begin{array}{c} 4\gamma^2\mu_0\left\{\begin{array}{c}(\beta_n-\alpha_n)\left(\begin{array}{c}\zeta_1(\gamma)[-2+2\nu_0-\gamma^2(2\nu_0-1)] \\ -4\gamma^2\zeta_2(\gamma)+4\zeta_3(\gamma)[1+\nu_0(\gamma^2-1)]\end{array}\right) \\ +\alpha_n(\zeta_4(\gamma)[-2+2\nu_0-\gamma^2(2\nu_0-1)]-4\gamma^2\zeta_5(\gamma))\end{array}\right\} \\ -g^2(\gamma)\left\{\begin{array}{c}(\beta_n-\alpha_n)(3\zeta_1(\gamma)\varsigma_{15}(\gamma)-4\zeta_2(\gamma)\varsigma_{16}(\gamma)-2\zeta_3(\gamma)\varsigma_{14}(\gamma)) \\ +\alpha_n(3\zeta_4(\gamma)\varsigma_{15}(\gamma)-4\zeta_5(\gamma)\varsigma_{16}(\gamma))\end{array}\right\} \\ +4g(\gamma)\left\{\begin{array}{c}(\beta_n-\alpha_n)(2\zeta_2(\gamma)\varsigma_{11}(\gamma)-\zeta_1(\gamma)\varsigma_{17}(\gamma)-\zeta_3(\gamma)\varsigma_{19}(\gamma)) \\ +\alpha_n(\zeta_5(\gamma)\varsigma_{11}(\gamma)-\zeta_4(\gamma)\varsigma_{17}(\gamma))\end{array}\right\} \end{array}\right] \tag{13}$$

$$S_{22}^{M(2n-1)} = S_{23}^{M(2n-1)} = S_{32}^{M(2n-1)} = S_{33}^{M(2n-1)} = S_{22}^{(1)} + \frac{3}{32a[1-\nu_0][\gamma^2-1]^2}$$
$$\left[\begin{array}{c} \varsigma_5(\gamma)\varsigma_6(\gamma)\{\zeta_1(\gamma)(\beta_n-\alpha_n)+2\alpha_n\zeta_4(\gamma)\} \\ +\{\mu_0\varsigma_5(\gamma)+\varsigma_6(\gamma)\}\left\{\begin{array}{c}(\alpha_n-\beta_n)(\zeta_1(\gamma)\varsigma_{18}(\gamma)+8\zeta_3(\gamma)\varsigma_8(\gamma)) \\ -2\alpha_n\zeta_4(\gamma)\varsigma_7(\gamma)\end{array}\right\} \\ +16\varsigma_{12}(\gamma)\{(\alpha_n-\beta_n)(\zeta_2(\gamma)\varsigma_8(\gamma)+\zeta_3(\gamma)\varsigma_{13}(\gamma))-2\alpha_n\zeta_5(\gamma)\varsigma_8(\gamma)\} \end{array}\right] \tag{14}$$

$$S_{11}^{M(2n)} = S_{11}^{(2)} + \frac{2\alpha_n\mu_0\zeta_5(\gamma)[1+3\varsigma_2(\gamma)]^2}{3a[1-\nu_0][\gamma^2-1]^2} \tag{15}$$

$$S_{12}^{M(2n)} = S_{13}^{M(2n)} = S_{21}^{M(2n)} = S_{31}^{M(2n)}$$
$$= S_{12}^{(2)} + \frac{3\mu_0\varsigma_{20}^2(\gamma)[4(\beta_n-\alpha_n)\zeta_3(\gamma)+\alpha_n(\zeta_4(\gamma)+2\zeta_5(\gamma))]}{8a[1-\nu_0][\gamma^2-1]^2} \tag{16}$$

$$S_{22}^{M(2n)} = S_{23}^{M(2n)} = S_{32}^{M(2n)} = S_{33}^{M(2n)}$$
$$= S_{22}^{(2)} + \frac{3\mu_0\varsigma_5^2(\gamma)[(\beta_n-\alpha_n)\zeta_1(\gamma)+2\alpha_n\zeta_4(\gamma))]}{128a[1-\nu_0][\gamma^2-1]^2} \quad (17)$$

where γ denotes the aspect ratio (a_1/a_2) of the reinforcements and $\varsigma_1(\gamma), \ldots, \varsigma_{20}(\gamma)$, $\zeta_1(\gamma), \ldots, \zeta_5(\gamma)$ and $g(\gamma)$ are listed in Appendix A.

Substituting Eqs. (2) and (10) into Eq. (1) yields the effective stiffness tensor $\mathbf{C}^*$ for the current five-phase composites containing aligned spheroidal reinforcements as

$$\mathbf{C}^* = \left[C_{IK}^{(1)}\delta_{ij}\delta_{kl} + C_{IJ}^{(2)}(\delta_{ik}\delta_{jl}+\delta_{il}\delta_{jk})\right] \quad (18)$$

where

$$C_{IK}^{(1)} = 2\lambda_0\chi_{KK}^{(2)} + 2\mu_0\chi_{IK}^{(1)} + \sum_{n=1}^{3}\lambda_0\chi_{nK}^{(1)}, \quad C_{IJ}^{(2)} = 2\mu_0\chi_{IJ}^{(2)} \quad (19)$$

in which λ_0 denotes the Lame constant of the matrix, and the components $\chi_{IK}^{(1)}$ and $\chi_{IJ}^{(2)}$ are given by

$$\chi_{IK}^{(1)} = \Lambda_{IK}^{(1)} + \Lambda_{IK}^{(3)} + \Lambda_{IK}^{(5)} + \Lambda_{IK}^{(7)}, \quad \chi_{IJ}^{(2)} = \frac{1}{2} + \Lambda_{IJ}^{(2)} + \Lambda_{IJ}^{(4)} + \Lambda_{IJ}^{(6)} + \Lambda_{IJ}^{(8)} \quad (20)$$

where

$$\Lambda_{IK}^{(2r-1)} = \phi_r\left[2\eta_{IK}^{(2r-1)}\omega_{KK}^{(2r)} + 2\eta_{II}^{(2r)}\omega_{IK}^{(2r-1)} + \sum_{n=1}^{3}\eta_{In}^{(2r-1)}\omega_{nK}^{(2r-1)}\right] \quad (r=1,2,3,4) \quad (21)$$

$$\Lambda_{IJ}^{(2r)} = 2\phi_r\eta_{IJ}^{(2r)}\omega_{IJ}^{(2r)} \quad (r=1,2,3,4) \quad (22)$$

and

$$\omega_{IK}^{(2r-1)} = \frac{\Gamma_{IK}^{(r)}}{1-2\xi_{II}^{(2r)}}, \quad \omega_{IJ}^{(2r)} = \frac{1}{2-4\xi_{IJ}^{(2r)}} \quad (23)$$

$$\Gamma_{I1}^{(r)} = \frac{\left[\frac{1}{2}-\xi_{22}^{(2r-1)}-\xi_{22}^{(2r)}\right]\xi_{I1}^{(2r-1)} + \xi_{21}^{(2r-1)}\xi_{I2}^{(2r-1)}}{\left[\frac{1}{2}-\xi_{22}^{(2r-1)}-\xi_{22}^{(2r)}\right]\left[1-\xi_{11}^{(2r-1)}-2\xi_{11}^{(2r)}\right] - \xi_{12}^{(2r-1)}\xi_{21}^{(2r-1)}} \quad (24)$$

$$\Gamma_{I2}^{(r)} = \Gamma_{I3}^{(r)} = \frac{\left[1-\xi_{11}^{(2r-1)}-2\xi_{11}^{(2r)}\right]\xi_{I2}^{(2r-1)} + \xi_{12}^{(2r-1)}\xi_{I1}^{(2r-1)}}{2\left[\frac{1}{2}-\xi_{22}^{(2r-1)}-\xi_{22}^{(2r)}\right]\left[1-\xi_{11}^{(2r-1)}-2\xi_{11}^{(2r)}\right] - 2\xi_{12}^{(2r-1)}\xi_{21}^{(2r-1)}} \quad (25)$$

Here, the parameters $\xi_{IK}^{(1)}$, $\xi_{IJ}^{(2)}$, …, $\xi_{IK}^{(7)}$, $\xi_{IJ}^{(8)}$, and $\eta_{IK}^{(1)}$, $\eta_{IJ}^{(2)}$, …, $\eta_{IK}^{(7)}$, $\eta_{IJ}^{(8)}$ are listed in Appendix B.

3 Effective elastic moduli of composites containing randomly oriented spheroidal reinforcements

One may apply the orientational averaging process (suitable for aligned to 3D random orientation) to the effective elastic moduli of composites with aligned spheroidal reinforcements in order to obtain the effective elastic moduli of composites with randomly oriented spheroidal reinforcements. Any transversely isotropic fourth-rank tensor $\mathbf{M}$ can be expressed as

$$M_{ijkl} = M_{IK}^{(1)} \delta_{ij}\delta_{kl} + M_{IJ}^{(2)} (\delta_{ik}\delta_{jl} + \delta_{il}\delta_{jk}) \tag{26}$$

where $M_{12}^{(1)} = M_{13}^{(1)}$, $M_{21}^{(1)} = M_{31}^{(1)}$, $M_{22}^{(1)} = M_{23}^{(1)} = M_{32}^{(1)} = M_{33}^{(1)}$, $M_{12}^{(2)} = M_{21}^{(2)} = M_{13}^{(2)} = M_{31}^{(2)}$, and $M_{22}^{(2)} = M_{23}^{(2)} = M_{32}^{(2)} = M_{33}^{(2)}$.

The general orientation average process proposed by Marzari and Ferrari (1992) and Odegard, Gates, Wise, Park, and Siochi (2003) can be written as

$$\ll \mathbf{M} \gg = \frac{\int_{-\pi}^{\pi}\int_{0}^{\pi}\int_{0}^{\pi/2} \bar{M}(\phi,\gamma,\psi)\lambda(\phi,\psi)\sin\gamma d\phi d\gamma d\psi}{\int_{-\pi}^{\pi}\int_{0}^{\pi}\int_{0}^{\pi/2} \lambda(\phi,\psi)\sin\gamma d\phi d\gamma d\psi} \tag{27}$$

where $\ll \cdot \gg$ is used to define the orientational average process and $\bar{M}_{ijkl} = c_{ip}c_{jq}c_{kr}c_{ls}M_{pqrs}$, in which c_{ij} are the direction cosines for the transformation and listed in Eq. (27) of Odegard, Gates, Wise, Park, and Siochi (2003). Eq. (27) in the case of 3D random orientation can be simplified as [Marzari and Ferrari (1992); Odegard, Gates, Wise, Park, and Siochi (2003)]

$$\ll \mathbf{M} \gg = \frac{\int_{-\pi}^{\pi}\int_{0}^{\pi}\int_{0}^{\pi/2} \bar{M}(\phi,\gamma,\psi)\sin\gamma d\phi d\gamma d\psi}{\int_{-\pi}^{\pi}\int_{0}^{\pi}\int_{0}^{\pi/2} \sin\gamma d\phi d\gamma d\psi} \tag{28}$$

After lengthy but straightforward algebra, $\ll \mathbf{M} \gg$ becomes

$$\ll \mathbf{M} \gg = \iota_1 \delta_{ij}\delta_{kl} + \iota_2(\delta_{ik}\delta_{jl} + \delta_{il}\delta_{jk}) \tag{29}$$

where

$$\iota_1 = \frac{1}{15}\left[M_{11}^{(1)} + 4M_{12}^{(1)} + 4M_{21}^{(1)} + 6M_{22}^{(1)} + 2M_{11}^{(2)} - 4M_{12}^{(2)} + 2M_{22}^{(2)}\right] \tag{30}$$

$$\iota_2 = \frac{1}{15}\left[M_{11}^{(1)} - M_{12}^{(1)} - M_{21}^{(1)} + M_{22}^{(1)} + 2M_{11}^{(2)} + 6M_{12}^{(2)} + 7M_{22}^{(2)}\right] \tag{31}$$

Firstly, we adopt here Lee and Simunovic (2000)'s approach to obtain the effective elastic moduli of composites with 3D randomly oriented reinforcements. Following

Lee and Simunovic (2000), the effective stiffness tensor $\mathbf{C}^*$ for composites containing randomly oriented spheroidal can be written as [Lee and Simunovic (2000)]

$$\mathbf{C}^* = \left\langle\left\langle \mathbf{C}_0 \cdot \left\{ \mathbf{I} + \sum_{r=1}^{4} \left[\phi_r (\mathbf{A}_r + \mathbf{S}_r)^{-1} \cdot \{ \mathbf{I} - \phi_r \mathbf{S}_r \cdot (\mathbf{A}_r + \mathbf{S}_r)^{-1} \}^{-1} \right] \right\} \right\rangle\right\rangle = \tilde{C}_1 \delta_{ij}\delta_{kl} + \tilde{C}_2 (\delta_{ik}\delta_{jl} + \delta_{il}\delta_{jk}) \quad (32)$$

where

$$\tilde{C}_1 = \frac{1}{15}\left[C_{11}^{(1)} + 4C_{12}^{(1)} + 4C_{21}^{(1)} + 6C_{22}^{(1)} + 2C_{11}^{(2)} - 4C_{12}^{(2)} + 2C_{22}^{(2)} \right] \quad (33)$$

$$\tilde{C}_2 = \frac{1}{15}\left[C_{11}^{(1)} - C_{12}^{(1)} - C_{21}^{(1)} + C_{22}^{(1)} + 2C_{11}^{(2)} + 6C_{12}^{(2)} + 7C_{22}^{(2)} \right] \quad (34)$$

where the components $C_{11}^{(1)}$, $C_{12}^{(1)}$, $C_{21}^{(1)}$, $C_{22}^{(1)}$, $C_{11}^{(2)}$, $C_{12}^{(2)}$ and $C_{22}^{(2)}$ are given in Eq. (19).

In accordance with Sun and Ju (2004)'s approach for the 3D random orientation, the effective elastic stiffness tensor $\mathbf{C}^*$ for composites with randomly oriented spheroidal reinforcements can be alternatively given by [Sun and Ju (2004)]

$$\mathbf{C}^* = \mathbf{C}_0 \cdot \left\{ \mathbf{I} + \sum_{r=1}^{4} \phi_r \left[\ll (\mathbf{A}_r + \mathbf{S}_r)^{-1} \gg \right] \cdot \left[\mathbf{I} - \phi_r \ll \mathbf{S}_r \cdot (\mathbf{A}_r + \mathbf{S}_r)^{-1} \gg \right]^{-1} \right\} \quad (35)$$

After lengthy algebra, the effective elastic stiffness tensor of the composites can be rephrased as

$$\mathbf{C}^* = \lambda^* \delta_{ij}\delta_{kl} + \mu^* (\delta_{ik}\delta_{jl} + \delta_{il}\delta_{jk}) \quad (36)$$

where

$$\lambda^* = [3\lambda_0 + 2\mu_0][\psi_1 + \psi_3 + \psi_5 + \psi_7] + \lambda_0[1 + 2\psi_2 + 2\psi_4 + 2\psi_6 + 2\psi_8] \quad (37)$$

$$\mu^* = \mu_0[1 + 2\psi_2 + 2\psi_4 + 2\psi_6 + 2\psi_8] \quad (38)$$

with

$$\psi_{2r-1} = \frac{\phi_r \Theta_{2r-1} + 2\phi_r^2[\Upsilon_{2r-1}\Theta_{2r} - \Upsilon_{2r}\Theta_{2r-1}]}{[1 - 2\phi_r\Upsilon_{2r}][1 - 3\phi_r\Upsilon_{2r-1} - 2\phi_r\Upsilon_{2r}]},\ \psi_{2r} = \frac{\phi_r\Theta_{2r}}{1 - 2\phi_r\Upsilon_{2r}},\ (r = 1,2,3,4) \quad (39)$$

in which the parameters $\Upsilon_1, \ldots, \Upsilon_8$ and $\Theta_1, \ldots, \Theta_8$ are listed in Appendix C.

Lastly, one may also adopt Qiu and Weng (1990)'s approach for the 3D random orientation based on the Mori-Tanaka method. The effective elastic stiffness tensor $\mathbf{C}^*$ for composites with randomly oriented spheroidal reinforcements can thus be written as [Qiu and Weng (1990)]

$$\mathbf{C}^* = \left[(1-\phi)\mathbf{C}_0 + \sum_{r=1}^{4} \phi_r \ll \mathbf{C}_r \cdot \mathbf{B}_r \gg\right] \left[(1-\phi)\mathbf{I} + \sum_{r=1}^{4} \phi_r \ll \mathbf{B}_r \gg\right]^{-1} \tag{40}$$

where

$$\mathbf{B}_r = \left[\mathbf{I} + \mathbf{S}_r(\mathbf{C}_0)^{-1}(\mathbf{C}_r - \mathbf{C}_0)\right]^{-1} \tag{41}$$

After lengthy algebra, the effective elastic stiffness tensor read

$$\mathbf{C}^* = \lambda^* \delta_{ij}\delta_{kl} + \mu^*(\delta_{ik}\delta_{jl} + \delta_{il}\delta_{jk}) \tag{42}$$

where

$$\lambda^* = \frac{\left[\begin{array}{c} -\left[\Sigma_{n=1}^{4}\phi_n\varpi_{2n-1}\right]\left[(1-\phi)(3\lambda_0+2\mu_0)+2\Sigma_{n=1}^{3}\phi_n\rho_{2n}\right] \\ +\left[1-\phi+2\Sigma_{n=1}^{4}\phi_n\varpi_{2n}\right]\left[(1-\phi)\mu_0+\Sigma_{n=1}^{3}\phi_n\rho_{2n-1}\right] \end{array}\right]}{\left[1-\phi+2\Sigma_{n=1}^{4}\phi_n\varpi_{2n}\right]\left[1-\phi+\Sigma_{n=1}^{4}\phi_n(3\varpi_{2n-1}+2\varpi_{2n})\right]} \tag{43}$$

$$\mu^* = \frac{(1-\phi)\mu_0 + \Sigma_{n=1}^{3}\phi_n\rho_{2n}}{1-\phi+2\Sigma_{n=1}^{4}\phi_n\varpi_{2n}} \tag{44}$$

with

$$\rho_1 = \frac{1-\nu_0}{15}\left[\begin{array}{c} \frac{\{5\lambda_1+2\mu_1\}\left\{1-\hat{\Psi}_{11}^{(1)}-2\hat{\Psi}_{12}^{(1)}\right\}-4\mu_1\hat{\Psi}_{12}^{(1)}}{1-\nu_0+\hat{\mu}_1 S_{11}^{(2)}-\frac{4\mu_1}{1-\nu_0+\hat{\mu}_1 S_{12}^{(2)}}} \\ +\frac{\{10\lambda_1+2\mu_1\}\left\{1-\hat{\Psi}_{21}^{(1)}-2\hat{\Psi}_{22}^{(1)}\right\}-6\mu_1\hat{\Psi}_{21}^{(1)}-8\mu_1\hat{\Psi}_{22}^{(1)}}{1-\nu_0+\hat{\mu}_1 S_{22}^{(2)}} \end{array}\right] \tag{45}$$

$$\rho_2 = \frac{\mu_1(1-\nu_0)}{15}\left[\frac{2\left\{1-\hat{\Psi}_{11}^{(1)}+\hat{\Psi}_{12}^{(1)}\right\}}{1-\nu_0+\hat{\mu}_1 S_{11}^{(2)}} + \frac{6}{1-\nu_0+\hat{\mu}_1 S_{12}^{(2)}} + \frac{7+2\hat{\Psi}_{21}^{(1)}-2\hat{\Psi}_{22}^{(1)}}{1-\nu_0+\hat{\mu}_1 S_{22}^{(2)}}\right] \tag{46}$$

$$\rho_3 = \frac{1-\nu_0}{15}\left[\begin{array}{c} \frac{\{5\lambda_2+2\mu_2\}\left\{1-\hat{\Psi}_{11}^{(2)}-2\hat{\Psi}_{12}^{(2)}\right\}-4\mu_2\hat{\Psi}_{12}^{(2)}}{1-\nu_0+\hat{\mu}_2 S_{11}^{M(2)}} - \frac{4\mu_2}{1-\nu_0+\hat{\mu}_2 S_{12}^{M(2)}} \\ +\frac{\{10\lambda_2+2\mu_2\}\left\{1-\hat{\Psi}_{21}^{(2)}-2\hat{\Psi}_{22}^{(2)}\right\}-6\mu_2\hat{\Psi}_{21}^{(2)}-8\mu_2\hat{\Psi}_{22}^{(2)}}{1-\nu_0+\hat{\mu}_2 S_{22}^{M(2)}} \end{array}\right] \tag{47}$$

$$\rho_4 = \frac{\mu_2(1-\nu_0)}{15}\left[\frac{2\left\{1-\hat{\Psi}_{11}^{(2)}+\hat{\Psi}_{12}^{(2)}\right\}}{1-\nu_0+\hat{\mu}_2 S_{11}^{M(2)}} + \frac{6}{1-\nu_0+\hat{\mu}_2 S_{12}^{M(2)}} + \frac{7+2\hat{\Psi}_{21}^{(2)}-2\hat{\Psi}_{22}^{(2)}}{1-\nu_0+\hat{\mu}_2 S_{22}^{M(2)}}\right] \tag{48}$$

$$\rho_5 = \frac{1-\nu_0}{15}\left[\begin{array}{c}\dfrac{\{5\lambda_3+2\mu_3\}\left\{1-\hat{\Psi}_{11}^{(3)}-2\hat{\Psi}_{12}^{(3)}\right\}-4\mu_3\hat{\Psi}_{12}^{(3)}}{1-\nu_0+\hat{\mu}_3 S_{11}^{M(4)}}-\dfrac{4\mu_3}{1-\nu_0+\hat{\mu}_3 S_{12}^{M(4)}}\\ +\dfrac{\{10\lambda_3+2\mu_3\}\left\{1-\hat{\Psi}_{21}^{(3)}-2\hat{\Psi}_{22}^{(3)}\right\}-6\mu_3\hat{\Psi}_{21}^{(3)}-8\mu_3\hat{\Psi}_{22}^{(3)}}{1-\nu_0+\hat{\mu}_3 S_{22}^{M(4)}}\end{array}\right] \tag{49}$$

$$\rho_6 = \frac{\mu_3(1-\nu_0)}{15}\left[\frac{2\left\{1-\hat{\Psi}_{11}^{(3)}+\hat{\Psi}_{12}^{(3)}\right\}}{1-\nu_0+\hat{\mu}_3 S_{11}^{M(4)}}+\frac{6}{1-\nu_0+\hat{\mu}_3 S_{12}^{M(4)}}+\frac{7+2\hat{\Psi}_{21}^{(3)}-2\hat{\Psi}_{22}^{(3)}}{1-\nu_0+\hat{\mu}_3 S_{22}^{M(4)}}\right] \tag{50}$$

$$\varpi_1 = \frac{1-\nu_0}{15}\left[\frac{1-\hat{\Psi}_{11}^{(1)}-4\hat{\Psi}_{12}^{(1)}}{1-\nu_0+\hat{\mu}_1 S_{11}^{(2)}}-\frac{2}{1-\nu_0+\hat{\mu}_1 S_{12}^{(2)}}+\frac{1-4\hat{\Psi}_{21}^{(1)}-6\hat{\Psi}_{22}^{(1)}}{1-\nu_0+\hat{\mu}_1 S_{22}^{(2)}}\right] \tag{51}$$

$$\varpi_2 = \frac{1-\nu_0}{30}\left[\frac{2-2\hat{\Psi}_{11}^{(1)}+2\hat{\Psi}_{12}^{(1)}}{1-\nu_0+\hat{\mu}_1 S_{11}^{(2)}}+\frac{6}{1-\nu_0+\hat{\mu}_1 S_{12}^{(2)}}+\frac{7+2\hat{\Psi}_{21}^{(1)}-2\hat{\Psi}_{22}^{(1)}}{1-\nu_0+\hat{\mu}_1 S_{22}^{(2)}}\right] \tag{52}$$

$$\varpi_3 = \frac{1-\nu_0}{15}\left[\frac{1-\hat{\Psi}_{11}^{(2)}-4\hat{\Psi}_{12}^{(2)}}{1-\nu_0+\hat{\mu}_2 S_{11}^{M(2)}}-\frac{2}{1-\nu_0+\hat{\mu}_2 S_{12}^{M(2)}}+\frac{1-4\hat{\Psi}_{21}^{(2)}-6\hat{\Psi}_{22}^{(2)}}{1-\nu_0+\hat{\mu}_2 S_{22}^{M(2)}}\right] \tag{53}$$

$$\varpi_4 = \frac{1-\nu_0}{30}\left[\frac{2-2\hat{\Psi}_{11}^{(2)}+2\hat{\Psi}_{12}^{(2)}}{1-\nu_0+\hat{\mu}_2 S_{11}^{M(2)}}+\frac{6}{1-\nu_0+\hat{\mu}_2 S_{12}^{M(2)}}+\frac{7+2\hat{\Psi}_{21}^{(2)}-2\hat{\Psi}_{22}^{(2)}}{1-\nu_0+\hat{\mu}_2 S_{22}^{M(2)}}\right] \tag{54}$$

$$\varpi_5 = \frac{1-\nu_0}{15}\left[\frac{1-\hat{\Psi}_{11}^{(3)}-4\hat{\Psi}_{12}^{(3)}}{1-\nu_0+\hat{\mu}_3 S_{11}^{M(4)}}-\frac{2}{1-\nu_0+\hat{\mu}_3 S_{12}^{M(4)}}+\frac{1-4\hat{\Psi}_{21}^{(3)}-6\hat{\Psi}_{22}^{(3)}}{1-\nu_0+\hat{\mu}_3 S_{22}^{M(4)}}\right] \tag{55}$$

$$\varpi_6 = \frac{1-\nu_0}{30}\left[\frac{2-2\hat{\Psi}_{11}^{(3)}+2\hat{\Psi}_{12}^{(3)}}{1-\nu_0+\hat{\mu}_3 S_{11}^{M(4)}}+\frac{6}{1-\nu_0+\hat{\mu}_3 S_{12}^{M(4)}}+\frac{7+2\hat{\Psi}_{21}^{(3)}-2\hat{\Psi}_{22}^{(3)}}{1-\nu_0+\hat{\mu}_3 S_{22}^{M(4)}}\right] \tag{56}$$

$$\varpi_7 = \frac{2(1-\nu_0)}{15}\left[\frac{1+\hat{\Psi}_{11}^{(4)}+4\hat{\Psi}_{12}^{(4)}}{2-2\nu_0-S_{11}^{(2)}}-\frac{2}{2-2\nu_0-S_{12}^{(2)}}+\frac{1+4\hat{\Psi}_{21}^{(4)}+6\hat{\Psi}_{22}^{(4)}}{2-2\nu_0-S_{22}^{(2)}}\right] \tag{57}$$

$$\varpi_8 = \frac{1-\nu_0}{15}\left[\frac{2+2\hat{\Psi}_{11}^{(4)}-2\hat{\Psi}_{12}^{(4)}}{2-2\nu_0-S_{11}^{(2)}}+\frac{6}{2-2\nu_0-S_{12}^{(2)}}+\frac{7-2\hat{\Psi}_{21}^{(4)}+2\hat{\Psi}_{22}^{(4)}}{2-2\nu_0-S_{22}^{(2)}}\right] \tag{58}$$

where the parameters $\hat{\Psi}_{IJ}^{(1)}, \ldots, \hat{\Psi}_{IJ}^{(4)}$ are listed in Appendix D.

4 Multi-level damage modeling and internal stress of reinforcements

A three-level damage model proposed in our preceding work [Lee and Pyo (2008a)] in the order of sequence of progressive imperfect interface is employed here to model the sequential, progressive imperfect interface in composites. The three-level damage model is briefly recapitulated in this section for completeness of the proposed model. Assuming that the Weibull (1951) statistics governs, as exter-

nal loads or deformations continue to increase, some initially perfectly bonded reinforcements are transformed statistically to reinforcements with mild imperfect interface (phase 2), some reinforcements with mild imperfect interface are then transformed to reinforcements with severe imperfect interface (phase 3), and all reinforcements are finally transformed to completely debonded reinforcements that are regarded as spheroidal voids (phase 4). Thus, the current volume fraction of r-phase reinforcements, ϕ_r, at a given level of $(\bar{\sigma}_{11})_1$ can be derived through the following three-step Weibull approach [Lee and Pyo (2008a)]

$$\bar{\phi}_2 = \phi \left\{ 1 - exp\left[-\left(\frac{(\bar{\sigma}_{11})_1}{S_0} \right)^M \right] \right\}, \quad \bar{\phi}_3 = \bar{\phi}_2 \left\{ 1 - exp\left[-\left(\frac{(\bar{\sigma}_{11})_1}{S_0} \right)^M \right] \right\} \tag{59}$$

$$\phi_4 = \bar{\phi}_3 \left\{ 1 - exp\left[-\left(\frac{(\bar{\sigma}_{11})_1}{S_0} \right)^M \right] \right\}, \;\; \phi_3 = \bar{\phi}_3 - \phi_4, \;\; \phi_2 = \bar{\phi}_2 - \bar{\phi}_3, \;\; \phi_1 = \phi - \bar{\phi}_2 \tag{60}$$

where ϕ denotes the original reinforcements volume fraction, $(\bar{\sigma}_{11})_1$ is the internal stress of reinforcements (phase 1) in the 1-direction, and S_0 and M are the Weibull parameters.

The internal stress of reinforcements required for the initiation of the imperfect interface for the multi-phase composite state can be explicitly derived as following [cf. Ju and Lee (2000); Lee and Pyo (2009)]

$$\bar{\boldsymbol{\sigma}}_1 \equiv \mathbf{U} : \bar{\boldsymbol{\varepsilon}} \tag{61}$$

with

$$U_{ijkl} = U_{IK}^{(1)} \delta_{ij} \delta_{kl} + U_{IJ}^{(2)} (\delta_{ik} \delta_{jl} + \delta_{il} \delta_{jk}) \tag{62}$$

where the second-rank tensors $U_{IK}^{(1)}$ and $U_{IJ}^{(2)}$ can be expressed as

$$U_{IK}^{(1)} = \frac{E_{IK}^{(1)}}{1 + 2\Pi_{KK}^{(2)}} - \frac{2E_{II}^{(2)} \Omega_{IK}}{1 + 2\Pi_{II}^{(2)}} - \sum_{n=1}^{3} \frac{E_{In}^{(1)} \Omega_{nK}}{1 + 2\Pi_{nn}^{(2)}}, \quad U_{IJ}^{(2)} = \frac{E_{IJ}^{(2)}}{1 + 2\Pi_{IJ}^{(2)}} \tag{63}$$

in which

$$E_{IK}^{(1)} = \lambda_1 \left[1 - \frac{2\xi_{KK}^{(2)}}{\phi_1} \right] - \frac{2\mu_1 \xi_{IK}^{(1)}}{\phi_1} - \frac{\lambda_1}{\phi_1} \sum_{n=1}^{3} \xi_{nK}^{(1)}, \quad E_{IJ}^{(2)} = \mu_1 \left[1 - \frac{2\xi_{IJ}^{(2)}}{\phi_1} \right] \tag{64}$$

with

$$\Omega_{I1} = \frac{\left[\frac{1}{2} + \Pi_{22}^{(1)} + \Pi_{22}^{(2)}\right]\Pi_{I1}^{(1)} - \Pi_{21}^{(1)}\Pi_{I2}^{(1)}}{\left[\frac{1}{2} + \Pi_{22}^{(1)} + \Pi_{22}^{(2)}\right]\left[1 + \Pi_{11}^{(1)} + 2\Pi_{11}^{(2)}\right] - \Pi_{12}^{(1)}\Pi_{21}^{(1)}} \tag{65}$$

$$\Omega_{I2} = \Omega_{I3} = \frac{\left[1 + \Pi_{11}^{(1)} + 2\Pi_{11}^{(2)}\right]\Pi_{I2}^{(1)} - \Pi_{12}^{(1)}\Pi_{I1}^{(1)}}{2\left[\frac{1}{2} + \Pi_{22}^{(1)} + \Pi_{22}^{(2)}\right]\left[1 + \Pi_{11}^{(1)} + 2\Pi_{11}^{(2)}\right] - 2\Pi_{12}^{(1)}\Pi_{21}^{(1)}} \tag{66}$$

and

$$\Pi_{IK}^{(1)} = -\left[\xi_{IK}^{(1)} + \xi_{IK}^{(3)} + \xi_{IK}^{(5)} + \xi_{IK}^{(7)}\right], \quad \Pi_{IJ}^{(2)} = -\left[\xi_{IJ}^{(2)} + \xi_{IJ}^{(4)} + \xi_{IJ}^{(6)} + \xi_{IJ}^{(8)}\right] \tag{67}$$

where the parameters $\xi_{IK}^{(1)}, \ldots, \xi_{IJ}^{(8)}$ in Eqs. (64) and (67) are listed in Appendix B.

5 Predictions for aligned whisker- or short fiber-reinforced composites

A series of numerical simulations are conducted to examine the influence of the Weibull parameters S_0 and M and the aspect ratio γ on the progression of imperfect interface and elastic behavior of aligned whisker- or short fiber-reinforced composites. We adopt the same material properties of SiC whisker-reinforced Al_2O_3 matrix composites as reported by Sudarsana Rao, Ghorpade, and Mukherjee (2006): E_0 = 400 GPa, ν_0 = 0.22, E_1 = 600 GPa, ν_1 = 0.22, ϕ = 0.33, γ = 200.0. Four sets of the Weibull parameters that are closely related to the strength at the fiber-matrix interface in the composites are used: S_0 = 200 MPa, M = 2.0; S_0 = 400 MPa, M = 2.0; S_0 = 600 MPa, M = 2.0; S_0 = 800 MPa, M = 2.0 in an attempt to investigate the effect of these parameters on the progression of imperfect interfaces. The compliance parameters explained in our preceding works [Lee and Pyo (2008a, 2009)] are assume to be $\alpha_1 = 2.0\times10^{-7}$, $\beta_1 = 3.0\times10^{-7}$, α_2 = 2.0, β_2 = 3.0.

Figure 3 shows the predicted elastic stress-strain responses of the composites at the five-phase composite state under the uniaxial tension with various S_0 values. Clearly, higher interfacial strength parameter S_0 is shown to lead to higher stress-strain responses. It is also found from this parametric analysis that the influence of the Weibull parameter S_0 on the stress-strain response is quite substantial. Figure 4 shows the predicted progression of volume fractions of reinforcements corresponding to Figure 3.

In order to evaluate the proposed elastic multi-level damage model sensitivity to the aspect ratio γ, a parametric analysis of γ is carried out. First, we consider the prolate spheroids case ($a_1 > a_2 = a_3$) with five sets of the aspect ratio as: γ = 2.0, γ = 3.0, γ = 5.0, γ = 10.0 and γ = 100.0. The values of Weibull and compliance

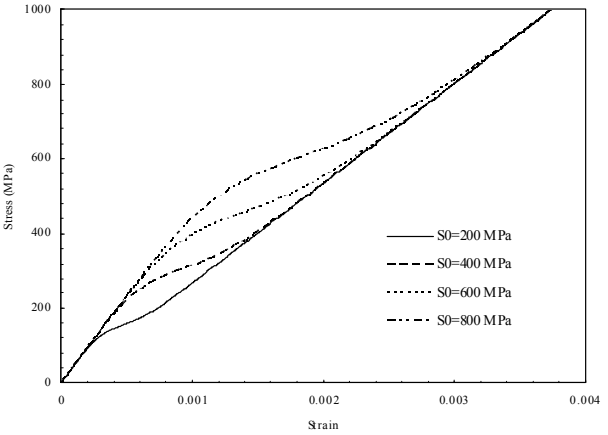

Figure 3: The predicted stress-strain responses of whisker-reinforced composites under uniaxial tension with various S_0 values

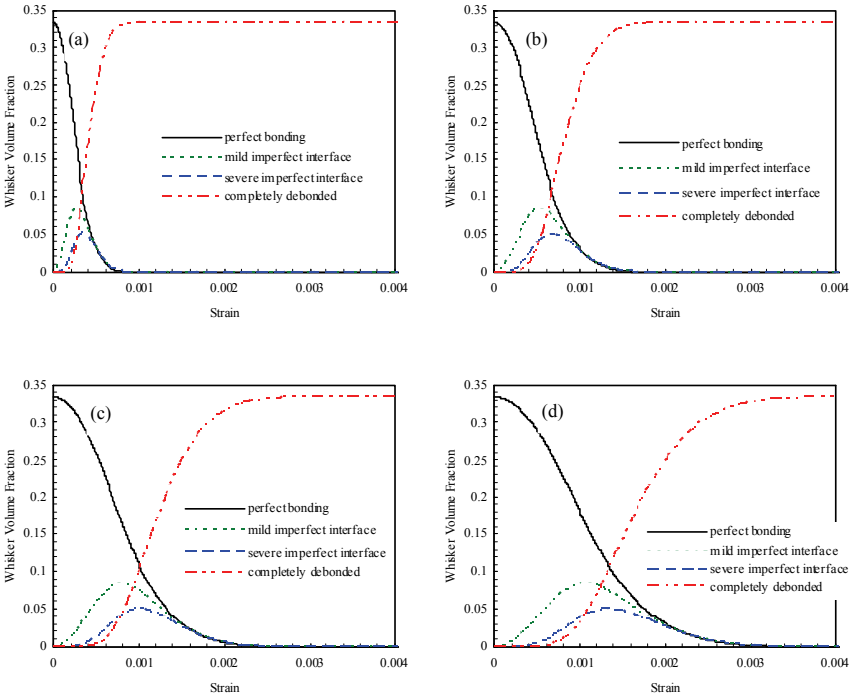

Figure 4: The predicted evolution of volume fractions of perfectly bonded whiskers, whiskers with mild imperfect interface, whiskers with severe imperfect interface, and completely debonded whiskers corresponding to the prediction in Figure 3: (a) $S_0 = 200$ MPa; (b) $S_0 = 400$ MPa; (c) $S_0 = 600$ MPa; (d) $S_0 = 800$ MPa

parameters are fixed to be $S_0 = 300$ MPa, $M = 2.0$; $\alpha_1 = 2.0 \times 10^{-7}$, $\beta_1 = 3.0 \times 10^{-7}$, $\alpha_2 = 2.0$, $\beta_2 = 3.0$. The predicted stress-strain responses of composites with various values of the aspect ratio γ ($\gamma > 1.0$) under the uniaxial tension are shown in Figure 5. It is seen from the figure that the effect of the aspect ratio γ on the stress-strain behavior of the composites become more influential, resulting in stiffer stress-strain curves, as γ continues to increase.

We also consider oblate spheroids case ($a_1 < a_2 = a_3$) with five sets of the aspect ratio as: $\gamma = 0.2$, $\gamma = 0.4$, $\gamma = 0.6$, $\gamma = 0.8$ and $\gamma = 0.9$. The same values of the Weibull and compliance parameters as used in the case of prolate spheroids case are used. Figure 6 depicts the predicted stress-strain responses of composites with various values of the aspect ratio γ ($\gamma < 1.0$) under the uniaxial tension. It is noted from the figure that higher stress-strain responses are obtained and the stress-strain curves converge to that of the spherical reinforcements ($\gamma = 1.0$) as γ continues to increase.

6 Predictions for randomly oriented whisker- or short fiber-reinforced composites

Predictions on randomly oriented whisker- or short fiber-reinforced composites are made to show the applicability of the proposed micromechanical approach for 3D randomly oriented reinforcements and to examine the influence of the aspect ratio γ on the composite behavior. Figures 7 - 9 show the predicted stress-strain responses of composites with 3D randomly oriented whiskers with various aspect ratio under uniaxial tension using the aforementioned three different orientational averaging approaches in Section 3. Figure 10 shows the comparison of predictions on aligned and randomly oriented whisker-reinforced composites. It is noted from the figures that the influence of the aspect ratio γ on the stress-strain response of composites is more pronounced with the aligned orientation. It is also observed from the figures that reinforcements with a smaller aspect ratio result in a higher stress-strain responses in the case of 3D random orientation case, which is opposite to the aligned orientation case.

7 Experimental comparison

Comparisons between the present predictions and experimental data on short glass fiber-reinforced polypropylene matrix composites [Fu, Lauke, Mäder, Yue, and Hu (2000)] and TiB whiskers reinforced Ti-6Al-4V matrix composites [Gorsse and Micracle (2003)] are made to highlight the predictive capability of the proposed model (in the cases of aligned and 3D random orientations).

First, we adopt the same material properties of the short glass fiber-reinforced

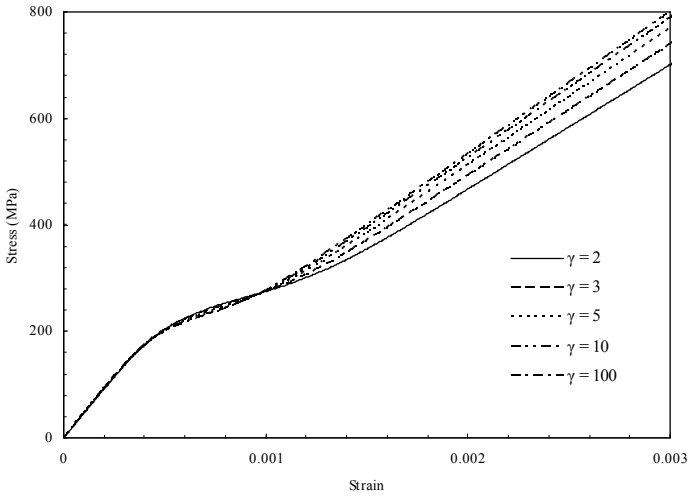

Figure 5: The predicted stress-strain responses of whisker-reinforced composites under uniaxial tension with various γ values ($\gamma > 1$)

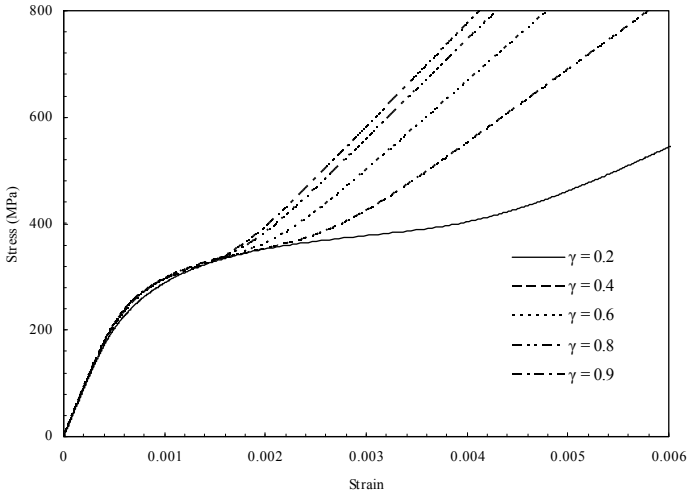

Figure 6: The predicted stress-strain responses of whisker-reinforced composites under uniaxial tension with various γ values ($\gamma < 1$)

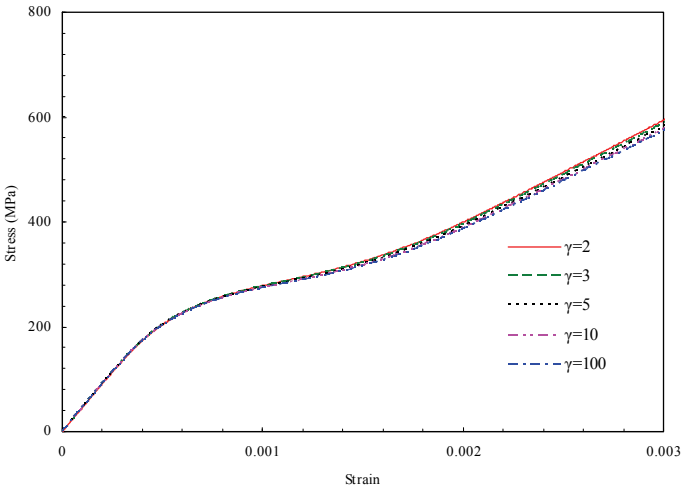

Figure 7: The predicted stress-strain responses of composites with randomly oriented whiskers under uniaxial tension with various γ values ($\gamma > 1$) using Lee and Simunovic (2000)'s approach

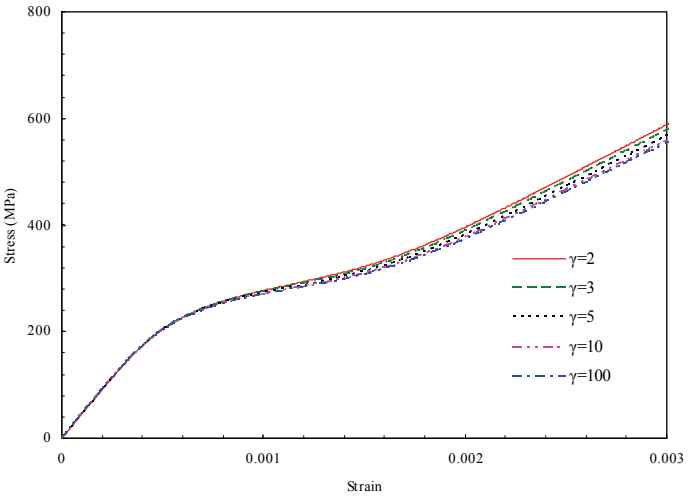

Figure 8: The predicted stress-strain responses of composites with randomly oriented whiskers under uniaxial tension with various γ values ($\gamma > 1$) using Sun and Ju (2004)'s approach

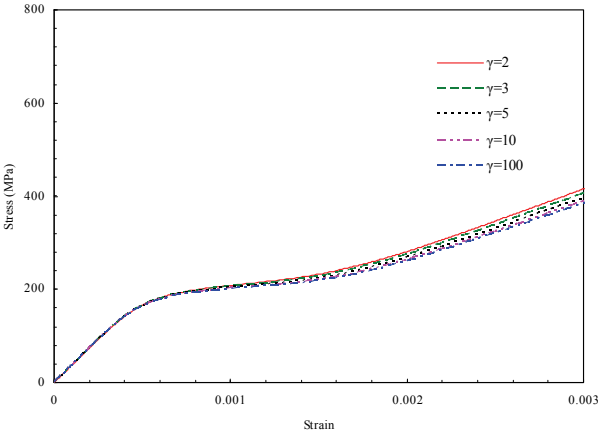

Figure 9: The predicted stress-strain responses of composites with random oriented whiskers under uniaxial tension with various γ values ($\gamma > 1$) using Qiu and Weng (1990)'s approach

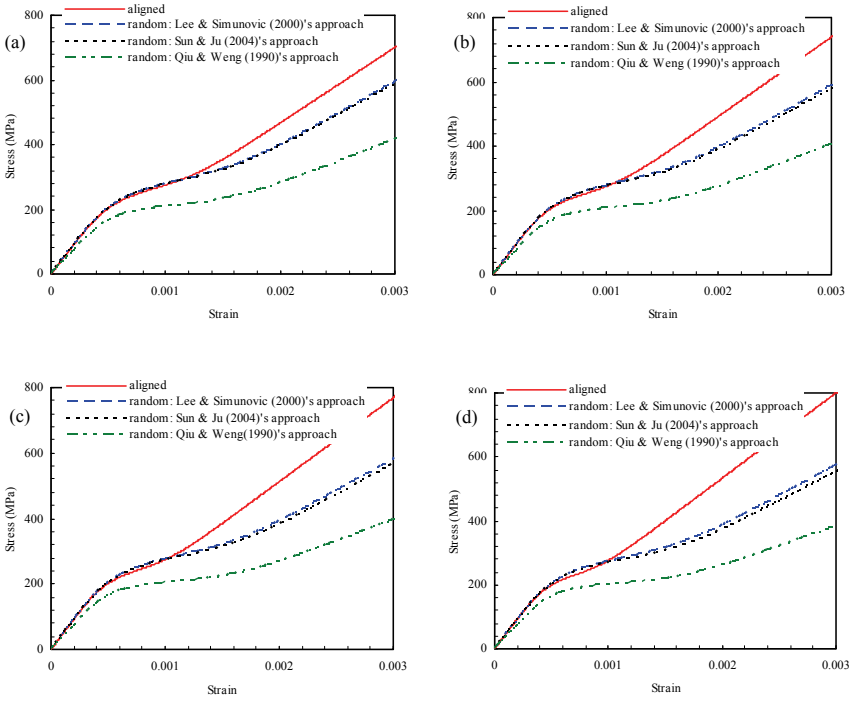

Figure 10: The comparison of predictions on aligned and randomly oriented whisker-reinforced composites: (a) $\gamma = 2$; (b) $\gamma = 3$; (c) $\gamma = 5$; (d) $\gamma = 100$

polypropylene matrix composites as those in Fu, Lauke, Mäder, Yue, and Hu (2000) and Fu, Xu, and Mai (2002) as: E_0 = 1.30 GPa, E_1 = 78.51 GPa, ν_1 = 0.25, ϕ = 0.25. The Poisson's ratio of the polypropylene matrix is assumed in accordance with Li, Jia, Mamtimin, Jiang, and An (2006) as ν_0 = 0.36. Since the model parameters of the proposed model were not reported by Fu, Lauke, Mäder, Yue, and Hu (2000), the model parameters are estimated by fitting the experimentally obtained stress-strain curve [Fu, Lauke, Mäder, Yue, and Hu (2000)] to the present prediction. The fitted model parameters are: $\alpha_1 = 2.0 \text{ x } 10^{-7}$, $\beta_1 = 3.0 \times 10^{-7}$, α_2 = 2.0, β_2 = 3.0; S_0 = 120 MPa, M = 0.45. The predicted uniaxial stress-strain curve of the composites based on the above material properties and parameters is shown in Figure 11. The experimentally obtained stress-strain curve is also plotted in the figure for comparison. Overall, the present prediction and the experimental data match well. The predicted evolution of volume fractions of fibers corresponding to Figure 11 is shown in Figure 12.

To further demonstrate the applicability of the proposed micromechanical framework, the present prediction is also compared with experimental data reported by Gorsse and Micracle (2003) for the uniaxial stress-strain behavior of aligned and 3D randomly oriented TiB whiskers reinforced Ti-6Al-4V matrix composites. We adopt the material properties of the composites according to Gorsse and Micracle (2003) as: E_0 = 109 GPa, E_1 = 482 GPa, ϕ = 0.2. Since they did not provide the Poisson's ratio of each constituent of the composites, typical values of the Poisson's ratio of each constituent are used as ν_0 = 0.27 and ν_1 = 0.14 [see, Fan, Miodownik, Chandrasekaran, and Ward-Close (1994)]. The compliance and Weibull parameters are estimated by fitting the experimentally obtained stress-strain curves [Gorsse and Micracle (2003)] for aligned and 3D random orientation cases to the present predictions. The estimated compliance parameters for both aligned and 3D random orientation cases are $\alpha_1 = 2.0 \text{ x } 10^{-7}$, $\beta_1 = 3.0 \text{ x } 10^{-7}$, α_2 = 2.0 and β_2 = 3.0. The fitted Weibull parameters for the aligned case are S_0 = 3.2 GPa, M = 3.2, while those for Lee and Simunovic (2000)'s, Sun and Ju (2004)'s, and Qiu and Weng (1990)'s approaches are S_0 = 1.9 GPa, M = 3.2; S_0 = 1.9 GPa, M = 3.2; S_0 = 2.1 GPa, M = 2.2, respectively. Figure 13 shows comparisons between the present predictions and experimental data for overall uniaxial tensile responses of aligned and 3D randomly oriented TiB whiskers reinforced Ti-6Al-4V matrix composites. A good correlation between the present prediction and experiment data is observed with the aligned case, whereas a slight deviation is observed from the predicted stress-strain curve for the 3D random case using Qiu and Weng (1990)'s approach. The predicted progression of volume fractions of whiskers of the composites corresponding to Figure 13 is shown in Figure 14.

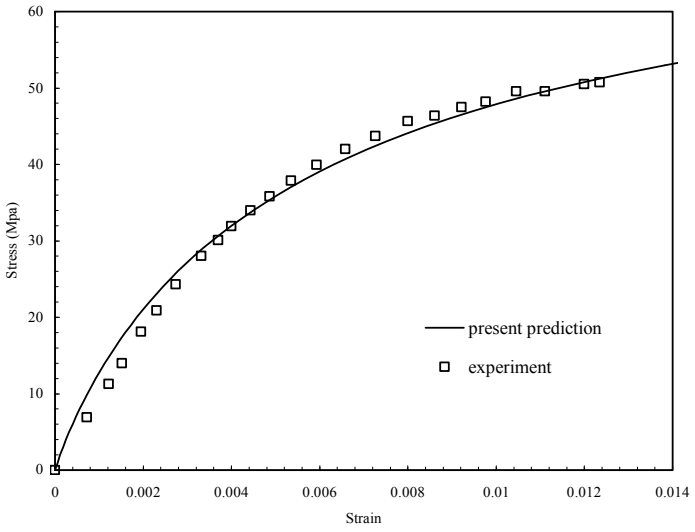

Figure 11: The comparison between the present prediction and experimental data (Fu et al., 2000) for overall uniaxial tensile responses of short glass fiber-reinforced polypropylene matrix composites

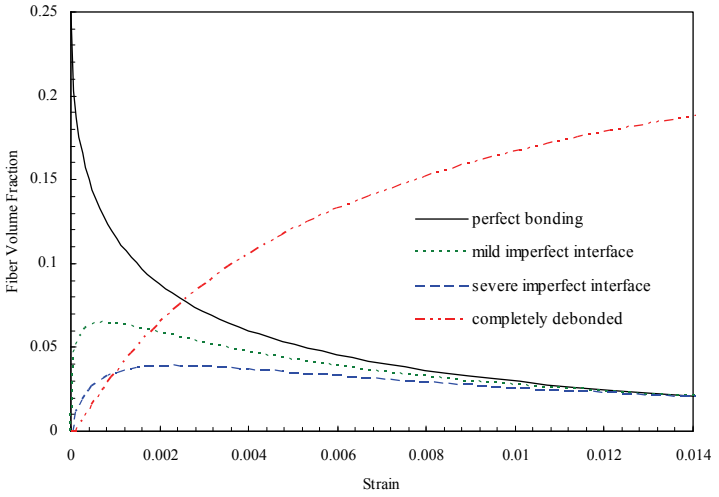

Figure 12: The predicted evolution of volume fractions of perfectly bonded fibers, fibers with mild imperfect interface, fibers with severe imperfect interface, and completely debonded fibers corresponding to the present prediction in Figure 11

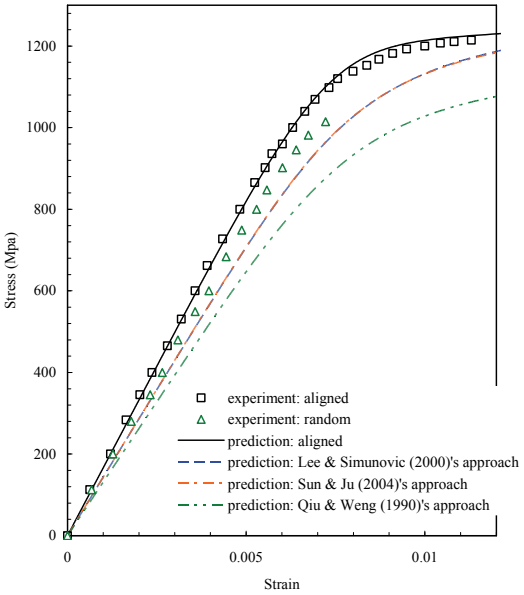

Figure 13: The comparison between the present predictions and experimental data (Gorsse and Miracle, 2003) for overall uniaxial tensile responses of aligned and 3D randomly oriented TiB whiskers reinforced Ti-6Al-4V matrix composites

8 Concluding remarks

In the present study, a micromechanical approach has been presented to predict the overall elastic and multi-level damage responses of composites with aligned and randomly oriented spheroidal reinforcements. Based on Eshelby's micromechanics and taking the evolutionary imperfect interface into consideration, the effective elastic moduli of the composites are obtained explicitly. The modified Eshelby's tensor for spheroidal inclusions with slightly weakened interface is extended to model reinforcements having mild or severe imperfect interfaces [Qu (1993a, b)]. Aligned and random orientations of spheroidal reinforcements are considered. A multi-level damage model [Lee and Pyo (2008a)] in accordance with the Weibull's probabilistic function is then incorporated into the elastic multi-level damage model to describe the sequential, progressive imperfect interface in the composites. Numerical examples corresponding to uniaxial tensile loadings are solved to illustrate the potential of the proposed micromechanical framework. Finally, comparisons between the present prediction and experimental data [Fu, Lauke, Mäder, Yue, and Hu (2000); Gorsse and Micracle (2003)] in the literature are conducted to highlight

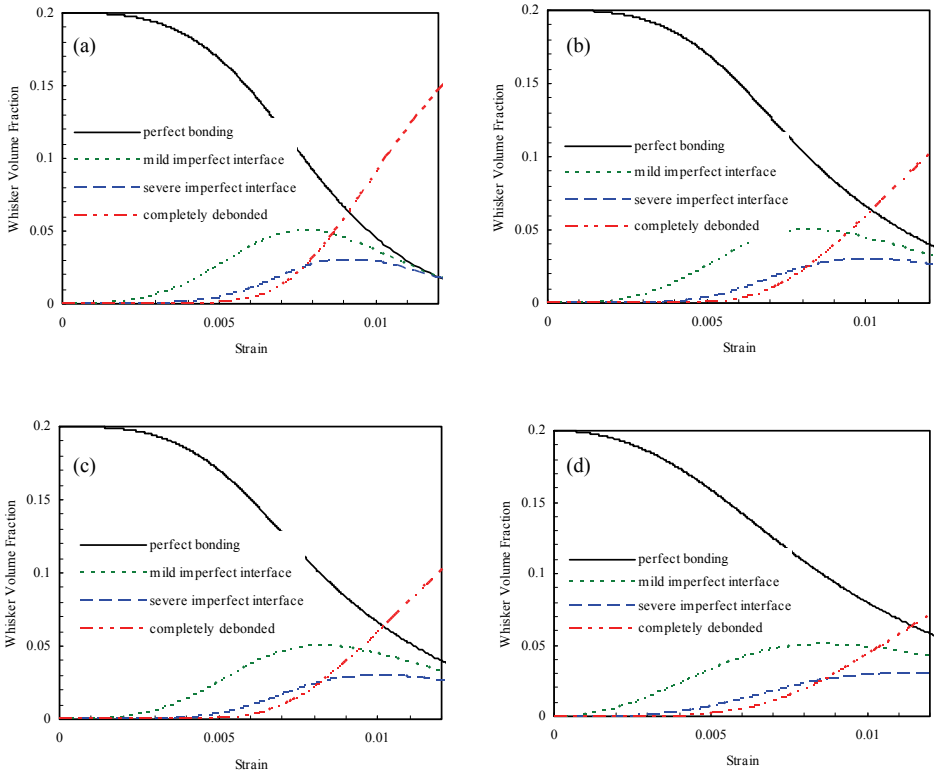

Figure 14: The predicted evolution of volume fractions of various states of whiskers corresponding to the present prediction in Figure 13: (a) aligned; (b) 3D random based on Lee and Simunovic (2001)'s approach; (c) 3D random based on Sun and Ju (2004)'s approach; (d) 3D random based on Qiu and Weng (1990)'s approach

the capability of the proposed micromechanical frameworks. The observations and findings of this numerical study can be summarized as:

(1) The modified Eshelby's tensor for spheroidal inclusion reinforced composites with imperfect interface is explicitly derived.

(2) Higher interfacial strength parameter S_0 is shown to slacken the damage evolution of reinforcements and leads to a higher stress-strain response.

(3) It is noted from the parametric studies on the aspect ratio γ for prolate spheroids ($a_1 > a_2 = a_3$) and oblate spheroids ($a_1 < a_2 = a_3$) cases that the influence of the aspect ratio γ on the stress-strain response of the composites is more influential in the case of oblate spheroids case than that of prolate spheroids case.

(4) Reinforcements with a smaller aspect ratio result in a higher stress-strain response in the case of 3D random orientation, which is opposite to the aligned orientation case.

(5) By using the fitted model parameters, the predicted stress-strain curves of composites with spheroidal reinforcements featuring the multi-level damage progression of imperfect interface is shown to be in good qualitative agreement with experimental data [Fu, Lauke, Mäder, Yue, and Hu (2000); Gorsse and Micracle (2003)] for both aligned and random orientation cases.

The proposed model will be extended to solve boundary value problems of chopped fiber-reinforced composite structures via implementation into a finite-element program. It is worth mentioning that the model parameters (e.g., compliance parameters) used in this work need to be calibrated through a series of experimentation on target composites for more realistic damage prediction of the composites.

Acknowledgement: This research was supported by a grant from Construction Technology Innovation Program(CTIP) funded by Ministry of Land, Transportation and Maritime Affairs (MLTM) of Korean government and IT R&D program of MKE/IITA (2008-F-044-01, Development of new IT convergence technology for smart building to improve the environment of electromagnetic waves, sound and building).

References

Arbelaiz, A.; Fernández, B.; Ramos, J. A.; Retegi, A.; Llano-Ponte, R.; Mondragon, I. (2005): Mechanical properties of short flax fibre bundle/polypropylene composites: Influence of matrix/fibre modification, fibre content, water uptake and recycling. *Composites Science and Technology*, vol. 65, pp. 1582-1592.

Chen, J.-T.; Ke, J.-N. (2008): Derivation of anti-plane dynamic green's function for several circular inclusions with imperfect interfaces. *CMES: Computer Modeling in Engineering Sciences*, vol. 29, pp. 111-135.

Fan, Z.; Miodownik, A. P.; Chandrasekaran, L.; Ward-Close, M. (1994): The Young's moduli of in situ Ti/TiB composites obtained by rapid solidification processing. *Journal of Materials Science*, vol. 29, pp. 1127-1134.

Fu, S.-Y.; Lauke, B.; Mäder, E.; Yue, C.-Y.; Hu, X. (2000): Tensile properties of short-glass-fiber- and short-carbon-fiber-reinforced polypropylene composites. *Composites Part A: Applied Science and Manufacturing*, vol. 31, pp. 1117-1125.

Fu, S.-Y.; Xu, G.; Mai, Y.-W. (2002): On the elastic modulus of hybrid particle/short-fiber/polymer composites. *Composites Part B: Engineering*, vol. 33, pp. 291-299.

Gao, Z. (1995): A circular inclusion with imperfect interface: Eshelby's tensor and related problems. *Journal of Applied Mechanics*, vol. 62, pp. 860-866.

Gorsse, S.; Miracle, D. B. (2003): Mechanical properties of Ti-6Al-4V/TiB composites with randomly oriented and aligned TiB reinforcements. *Acta Materialia*, vol. 51, pp. 2427-2442.

Hine, P. J.; Rudolf Lusti, H.; Gusev, A. A. (2002): Numerical simulation of the effects of volume fraction, aspect ratio and fibre length distribution on the elastic and thermoelastic properties of short fibre composites. *Composites Science and Technology*, vol. 62, pp. 1445-1453.

Huang, J. H. (2001): Some closed-form solutions for effective moduli of composites containing randomly oriented short fibers. *Materials Science and Engineering A*, vol. 315, pp. 11-20.

Joseph, K.; Thomas, S.; Pavithran, C. (1996): Effect of chemical treatment on the tensile properties of short sisal fibre-reinforced polyethylene composites. *Polymer*, vol. 37, pp. 5139-5149.

Ju, J. W.; Chen, T. M. (1994): Micromechanics and effective moduli of elastic composites containing randomly dispersed ellipsoidal inhomogeneities. *Acta Mechanica*, vol. 103, pp. 103-121.

Ju, J. W.; Lee, H. K. (2000): A micromechanical damage model for effective elastoplastic behavior of ductile matrix composites considering evolutionary complete particle debonding. *Computer Methods in Applied Mechanics and Engineering*, vol. 183, pp. 201-222.

Ju, J. W.; Sun, L. Z. (1999): A novel formulation for the exterior-point Eshelby's tensor of an ellipsoidal inclusion. *Journal of Applied Mechanics*, vol. 66, pp. 570-574.

Ju, J. W.; Sun, L. Z. (2001): Effective elastoplastic behavior of metal matrix composites containing randomly located aligned spheroidal inhomogeneities, Part I: micromechanics-based formulation. *International Journal of Solids and Structures*, vol. 38, pp. 183-201.

Lee, H. K.; Pyo, S. H. (2007): Micromechanics-based elastic damage modeling of particulate composites with weakened interfaces. *International Journal of Solids and Structures*, vol. 44, pp. 8390-8406.

Lee, H. K.; Pyo, S. H. (2008a): Multi-level modeling of effective elastic behavior and progressive weakened interface in particulate composites. *Composites Science and Technology*, vol. 68, pp. 387-397.

Lee, H. K.; Pyo, S. H. (2008b): An elastoplastic multi-level damage model for ductile matrix composites considering evolutionary weakened interface. *Interna-*

tional Journal of Solids and Structures, vol. 45, pp. 1614-1631.

Lee, H. K.; Pyo, S. H. (2009): A 3D-damage model for fiber-reinforced brittle composites with microcracks and imperfect interfaces. *Journal of Engineering Mechanics-ASCE*, doi. 10.1061/(ASCE)EM.1943-7889.0000039.

Lee, H. K.; Simunovic, S. (2000): Modeling of Progressive Damage in Aligned and Randomly Oriented Discontinuous Fiber Polymer Matrix Composites. *Composites Part B: Engineering*, vol. 31, pp. 77-86.

Lee, H. K.; Simunovic, S. (2001): A damage constitutive model of progressive debonding in aligned discontinuous fiber composites. *International Journal of Solids and Structures*, vol. 38, pp. 875-895.

Li, H.; Jia, Y.; Mamtimin, G.; Jiang, W.; An, L. (2006): Stress transfer and damage evolution simulations of fiber-reinforced polymer-matrix composites. *Materials Science and Engineering **A***, vol. 425, pp. 178-184.

Luo, J.; Stevens, R. (1996): Micromechanics of randomly oriented ellipsoidal inclusion composites. Part I: stress, strain and thermal expansion. *Journal of Applied Physics*, vol. 79, pp. 9047-9056.

Marzari, N.; Ferrari, M. (1992): Textural and micromorphological effects on the overall elastic response of macroscopically anisotropic composites. *Journal of Applied Mechanics*, vol. 59, pp. 269-275.

Maity, J.; Jacob, C.; Das, C. K.; Alam, S.; Singh, R. P. (2008): Direct fluorination of Twaron fiber and the mechanical, thermal and crystallization behaviour of short Twaron fiber reinforced polypropylene composites. *Composites Part A: Applied Science and Manufacturing*, vol. 31, pp. 1117-1125.

Mura, T. (1982): *Micromechanics of defects in solids*. Martinus Nijhoff, The Hague.

Nemat-Nasser, S.; Hori, M. (1993): *Micromechanics: Overall Properties of Heterogeneous Materials*. Elsevier, Amsterdam.

Nguyen, B. N.; Khaleel, M. A. (2004): A mechanistic approach to damage in short-fiber composites based on micromechanical and continuum damage mechanics descriptions. *Composites Science and Technology*, vol. 64, pp. 607-617.

Odegard, G. M.; Gates, T. S.; Wise, K. E.; Park, C.; Siochi, E. J. (2003): Constitutive modeling of nanotube-reinforced polymer composites. *Composites Science and Technology*, vol. 63, pp. 1671-1687.

Oyekoya, O. O.; Mba, D. U.; El-Zafrany, A. M. (2008): Structural integrity of functionally graded composite structure using mindlin-type element. *CMES: Computer Modeling in Engineering & Sciences*, vol. 34, pp. 55-85.

Pahr, D. H.; Böhm, H. J. (2008): Assessment of mixed uniform boundary condi-

tions for predicting the mechanical behavior of elastic and inelastic discontinuously reinforced composites. *CMES: Computer Modeling in Engineering & Sciences*, vol. 34, pp. 117-136.

Pyo, S. H.; Lee, H. K. (2009a): Micromechanics-based elastic-damage analysis of laminated composite structures. *International Journal of Solids and Structures*, in press.

Pyo, S. H.; Lee, H. K. (2009b): An elastoplastic damage model for metal matrix composites considering progressive imperfect interface under transverse loading. *International Journal of Plasticity*, submitted for publication.

Qiu, Y. P.; Weng, G. J. (1990): On the application of Mori-Tanaka's theory involving transversely isotropic spheroidal inclusions. *International Journal of Engineering Science*, vol. 28, pp. 1121-1137.

Qu, J. (1993a): Eshelby tensor for an elastic inclusion with slightly weakened interfaces. *Journal of Applied Mechanics*, vol. 60, pp. 1048-1050.

Qu, J. (1993b): The effect of slightly weakened interfaces on the overall elastic properties of composite materials. *Mechanics of Materials*, vol. 14, pp. 269-281.

Sudarsana Rao, H.; Ghorpade, V. G.; Mukherjee, A. (2006): A genetic algorithm based back propagation network for simulation of stress-strain response of ceramic-matrix-composites. *Computers and Structures*, vol. 84, pp. 330-339.

Sun, L. Z.; Ju, J. W. (2001): Effective elastoplastic behavior of metal matrix composites containing randomly located aligned spheroidal inhomogeneities, Part II: applications. *International Journal of Solids and Structures*, vol. 38, pp. 203-225.

Sun, L. Z.; Ju, J. W. (2004): Elastoplastic modeling of metal matrix composites containing randomly located and oriented spheroidal particles. *Journal of Applied Mechanics-ASME*, vol. 71, pp. 774-785.

Sun, L. Z.; Ju, J. W.; Liu, H. T. (2003): Elastoplastic modeling of metal matrix composites with evolutionary particle debonding. *Mechanics of Materials*, vol. 35, pp. 559-569.

Takashima, S.; Nakagaki, M.; Miyazaki, N. (2007): An elastic-plastic constitutive equation taking account of particle size and its application to a homogenized finite element analysis of a composite material. *CMES: Computer Modeling in Engineering & Sciences*, vol. 20, pp. 193-202.

Tucker III, C. L.; Liang, E. (1999): Stiffness predictions for unidirectional short-fiber composites: Review and evaluation. *Composites Science and Technology*, vol. 59, pp. 655-671.

Weibull, W. (1951): A statistical distribution function of wide applicability. *Jour-*

nal of Applied Mechanics, vol. 18, pp. 293-297.

Appendix A Parameters $\varsigma_1(\gamma), \ldots, \varsigma_{20}(\gamma)$, $\zeta_1(\gamma), \ldots, \zeta_5(\gamma)$ and $\mathbf{g}(\gamma)$ in Eqs. (11) – (17)

$$\varsigma_1(\gamma) = 2\gamma^2 + g(\gamma) + 2\gamma^2 g(\gamma) - 4\nu_0[1+g(\gamma)][\gamma^2-1] \tag{68}$$

$$\varsigma_2(\gamma) = g(\gamma)[1-2\nu_0+2\gamma^2(\nu_0-1)] - \nu_0 + \gamma^2[\nu_0-1] \tag{69}$$

$$\varsigma_3(\gamma) = 2\mu_0 + 3g(\gamma)[\mu_0+\lambda_0(\gamma^2-1)] + 6\nu_0[\gamma^2-1][\mu_0(1+g(\gamma)) - \lambda_0 g(\gamma)] \tag{70}$$

$$\varsigma_4(\gamma) = 2 + 3g(\gamma) + 6\nu_0[\gamma^2-1][1+g(\gamma)] \tag{71}$$

$$\varsigma_5(\gamma) = 8 + 7g(\gamma) - 6\gamma^2 - 4\gamma^2 g(\gamma) + 8\nu_0[\gamma^2-1][1+g(\gamma)] \tag{72}$$

$$\begin{aligned}\varsigma_6(\gamma) =& 4\lambda_0[2+g(\gamma)][\gamma^2-1][2\nu_0-1] \\ &+ \mu_0[2\gamma^2 + g(\gamma)\{-1+8\nu_0+4\gamma^2(1-2\nu_0)\}]\end{aligned} \tag{73}$$

$$\varsigma_7(\gamma) = -2\gamma^2 + g(\gamma)[1-8\nu_0+4\gamma^2(2\nu_0-1)] \tag{74}$$

$$\varsigma_8(\gamma) = 2\gamma^2 + g(\gamma)[1-2\nu_0+2\gamma^2(1+\nu_0)] \tag{75}$$

$$\varsigma_9(\gamma) = 2\gamma^2 - g(\gamma)[1-2\nu_0+2\gamma^2(\nu_0-2)] \tag{76}$$

$$\varsigma_{10}(\gamma) = 2\mu_0\gamma^2 + g(\gamma)[\mu_0\{1+2\gamma^2+2\nu_0(\gamma^2-1)\} + 2\lambda_0(\gamma^2-1)(2\nu_0-1)] \tag{77}$$

$$\varsigma_{11}(\gamma) = 2\gamma^2[\lambda_0(\gamma^2-1)(2\nu_0-1) - 6\mu_0\gamma^2] \tag{78}$$

$$\begin{aligned}\varsigma_{12}(\gamma) =& -\mu_0[g(\gamma) + 2\gamma^2(1+g(\gamma))] + 4\mu_0\nu_0[1+g(\gamma)][\gamma^2-1] \\ &+ \lambda_0[2+g(\gamma)][\gamma^2-1][2\nu_0-1]\end{aligned} \tag{79}$$

$$\varsigma_{13}(\gamma) = 4[\nu_0-1] + 2\gamma^2[1-2\nu_0] - 3g(\gamma) \tag{80}$$

$$\begin{aligned}\varsigma_{14}(\gamma) =& \lambda_0[\gamma^2-1][2\nu_0-1][-1-4\nu_0+4\gamma^2(1+\nu_0)] + 2\mu_0[-1+\nu_0+2\nu_0^2 \\ &+ 2\gamma^4(1+\nu_0)^2 + \gamma^2(8-5\nu_0-4\nu_0^2)]\end{aligned} \tag{81}$$

$$\varsigma_{15}(\gamma) = \mu_0 + 2[(1-\gamma^2)\lambda_0 + \gamma^2\mu_0 + \nu_0(\gamma^2-1)(2\lambda_0+\mu_0)] \tag{82}$$

$$\varsigma_{16}(\gamma) = [(1-\gamma^2)\lambda_0 + \mu_0 - 4\gamma^2\mu_0 + 2\nu_0(\gamma^2-1)(\lambda_0+\mu_0)][1-2\nu_0+2\gamma^2(1+\nu_0)] \tag{83}$$

$$\begin{aligned}\varsigma_{17}(\gamma) =& \mu_0 + \lambda_0[\gamma^2-1][2\nu_0-1][2-2\nu_0+\gamma^2(2\nu_0-1)] \\ &+ \mu_0[\gamma^2(1+\nu_0) - \nu_0][3-2\nu_0+\gamma^2(2\nu_0-1)]\end{aligned} \tag{84}$$

$$\varsigma_{18}(\gamma) = -8 - 5g(\gamma) + 2\gamma^2 - 4\gamma^2(\gamma) + 8\nu_0[g(\gamma)-1][\gamma^2-1] \tag{85}$$

$$\begin{aligned}\varsigma_{19}(\gamma) =& 2\mu_0[-1+\nu_0(\gamma^2-1)][1-2\nu_0+\gamma^2(2\nu_0-7)] \\ &+ \lambda_0[\gamma^2-1][2\nu_0-1][2-2\nu_0+\gamma^2(2\nu_0-3)]\end{aligned} \tag{86}$$

$$\varsigma_{20}(\gamma) = 2\gamma^2 + g(\gamma)[2-\nu_0+\gamma^2(1+\nu_0)] \tag{87}$$

with

$$\zeta_1(\gamma) = \int_0^{\pi} \gamma^3 \sin^5\varphi(\gamma^2\sin^2\varphi + \cos^2\varphi)^{-3/2} d\varphi \tag{88}$$

$$\zeta_2(\gamma) = \int_0^{\pi} \gamma^{-1} \cos^4\varphi \sin\varphi(\gamma^2\sin^2\varphi + \cos^2\varphi)^{-3/2} d\varphi \tag{89}$$

$$\zeta_3(\gamma) = \int_0^{\pi} \gamma \sin^3\varphi \cos^2\varphi(\gamma^2\sin^2\varphi + \cos^2\varphi)^{-3/2} d\varphi \tag{90}$$

$$\zeta_4(\gamma) = \int_0^{\pi} \gamma \sin^3\varphi(\gamma^2\sin^2\varphi + \cos^2\varphi)^{-1/2} d\varphi \tag{91}$$

$$\zeta_5(\gamma) = \int_0^{\pi} \gamma^{-1} \cos^2\varphi \sin\varphi(\gamma^2\sin^2\varphi + \cos^2\varphi)^{-1/2} d\varphi \tag{92}$$

$$g(\gamma) = \begin{cases} \frac{\gamma}{(1-\gamma^2)^{3/2}} \left[\gamma(1-\gamma^2)^{1/2} - \cos^{-1}\gamma\right], & \gamma < 1 \\ \frac{\gamma}{(\gamma^2-1)^{3/2}} \left[\cosh^{-1}\gamma - \gamma(\gamma^2-1)^{1/2}\right], & \gamma > 1 \end{cases} \tag{93}$$

Appendix B Parameters $\eta_{IK}^{(1)}$, $\eta_{IJ}^{(2)}$, …, $\eta_{IK}^{(7)}$, $\eta_{IJ}^{(8)}$ in Eqs. (21) and (22), $\xi_{IK}^{(1)}$, $\xi_{IJ}^{(2)}$, …, $\xi_{IK}^{(7)}$, $\xi_{IJ}^{(8)}$ in Eqs. (23) – (25), (64) and (67)

$$\xi_{IK}^{(1)} = \frac{\phi_1}{4(1-\nu_0)} \left[2S_{IK}^{(1)} \eta_{KK}^{(2)} + 2S_{II}^{(2)} \eta_{IK}^{(1)} + \sum_{n=1}^{3} S_{In}^{(1)} \eta_{nK}^{(1)} \right], \tag{94}$$

$$\xi_{IJ}^{(2)} = \frac{\phi_1 S_{IJ}^{(2)} \eta_{IJ}^{(2)}}{2(1-\nu_0)} \tag{95}$$

$$\xi_{IK}^{(3)} = \frac{\phi_2}{4(1-\nu_0)} \left[2S_{IK}^{M(1)} \eta_{KK}^{(4)} + 2S_{II}^{M(2)} \eta_{IK}^{(3)} + \sum_{n=1}^{3} S_{In}^{M(1)} \eta_{nK}^{(3)} \right], \tag{96}$$

$$\xi_{IJ}^{(4)} = \frac{\phi_2 S_{IJ}^{M(2)} \eta_{IJ}^{(4)}}{2(1-\nu_0)} \tag{97}$$

$$\xi_{IK}^{(5)} = \frac{\phi_3}{4(1-\nu_0)} \left[2S_{IK}^{M(3)} \eta_{KK}^{(6)} + 2S_{II}^{M(4)} \eta_{IK}^{(5)} + \sum_{n=1}^{3} S_{In}^{M(3)} \eta_{nK}^{(5)} \right], \tag{98}$$

$$\xi_{IJ}^{(6)} = \frac{\phi_3 S_{IJ}^{M(4)} \eta_{IJ}^{(6)}}{2(1-\nu_0)} \tag{99}$$

$$\xi_{IK}^{(7)} = \frac{\phi_4}{4(1-\nu_0)} \left[2S_{IK}^{(1)} \eta_{KK}^{(8)} + 2S_{II}^{(2)} \eta_{IK}^{(7)} + \sum_{n=1}^{3} S_{In}^{(1)} \eta_{nK}^{(7)} \right], \tag{100}$$

$$\xi_{IJ}^{(8)} = \frac{\phi_4 S_{IJ}^{(2)} \eta_{IJ}^{(8)}}{2(1-\nu_0)} \tag{101}$$

with

$$\eta_{IK}^{(1)} = -\frac{2(1-\nu_0)\Psi_{IK}^{(1)}}{\mu_1^{'} + S_{II}^{(2)}}, \qquad \eta_{IJ}^{(2)} = \frac{1-\nu_0}{\mu_1^{'} + S_{IJ}^{(2)}} \tag{102}$$

$$\eta_{IK}^{(3)} = -\frac{2(1-\nu_0)\Psi_{IK}^{(2)}}{\mu_2^{'} + S_{II}^{M(2)}}, \qquad \eta_{IJ}^{(4)} = \frac{1-\nu_0}{\mu_2^{'} + S_{IJ}^{M(2)}} \tag{103}$$

$$\eta_{IK}^{(5)} = -\frac{2(1-\nu_0)\Psi_{IK}^{(3)}}{\mu_3^{'} + S_{II}^{M(4)}}, \qquad \eta_{IJ}^{(6)} = \frac{1-\nu_0}{\mu_3^{'} + S_{IJ}^{M(4)}} \tag{104}$$

$$\eta_{IK}^{(7)} = -\frac{2(1-\nu_0)\Psi_{IK}^{(4)}}{-2(1-\nu_0) + S_{II}^{(2)}}, \qquad \eta_{IJ}^{(8)} = \frac{1-\nu_0}{-2(1-\nu_0) + S_{IJ}^{(2)}} \tag{105}$$

in which

$$\Psi_{I1}^{(1)} = \frac{\left[\lambda_1^{'} + \mu_1^{'} + S_{22}^{(1)} + S_{22}^{(2)}\right]\left[\lambda_1^{'} + S_{I1}^{(1)}\right] - \left[\lambda_1^{'} + S_{21}^{(1)}\right]\left[\lambda_1^{'} + S_{I2}^{(1)}\right]}{\left[\lambda_1^{'} + \mu_1^{'} + S_{22}^{(1)} + S_{22}^{(2)}\right]\left[\lambda_1^{'} + 2\mu_1^{'} + S_{11}^{(1)} + 2S_{11}^{(2)}\right] - \left[\lambda_1^{'} + S_{12}^{(1)}\right]\left[\lambda_1^{'} + S_{21}^{(1)}\right]} \tag{106}$$

$$\Psi_{I2}^{(1)} = \Psi_{I3}^{(1)} = \frac{\left[\lambda_1^{'} + 2\mu_1^{'} + S_{11}^{(1)} + 2S_{11}^{(2)}\right]\left[\lambda_1^{'} + S_{I2}^{(1)}\right] - \left[\lambda_1^{'} + S_{12}^{(1)}\right]\left[\lambda_1^{'} + S_{I1}^{(1)}\right]}{\left\{\begin{array}{c} 2\left[\lambda_1^{'} + \mu_1^{'} + S_{22}^{(1)} + S_{22}^{(2)}\right]\left[\lambda_1^{'} + 2\mu_1^{'} + S_{11}^{(1)} + 2S_{11}^{(2)}\right] \\ -2\left[\lambda_1^{'} + S_{12}^{(1)}\right]\left[\lambda_1^{'} + S_{21}^{(1)}\right] \end{array}\right\}} \tag{107}$$

$$\Psi_{I1}^{(2)} = \frac{\left[\lambda_2^{'} + \mu_2^{'} + S_{22}^{M(1)} + S_{22}^{M(2)}\right]\left[\lambda_2^{'} + S_{I1}^{M(1)}\right] - \left[\lambda_2^{'} + S_{21}^{M(1)}\right]\left[\lambda_2^{'} + S_{I2}^{M(1)}\right]}{\left\{\begin{array}{c} \left[\lambda_2^{'} + \mu_2^{'} + S_{22}^{M(1)} + S_{22}^{M(2)}\right]\left[\lambda_2^{'} + 2\mu_2^{'} + S_{11}^{M(1)} + 2S_{11}^{M(2)}\right] \\ -\left[\lambda_2^{'} + S_{12}^{M(1)}\right]\left[\lambda_2^{'} + S_{21}^{M(1)}\right] \end{array}\right\}} \tag{108}$$

$$\Psi_{I2}^{(2)} = \Psi_{I3}^{(2)} = \frac{\left\{\begin{array}{c} \left[\lambda_2^{'} + 2\mu_2^{'} + S_{11}^{M(1)} + 2S_{11}^{M(2)}\right]\left[\lambda_2^{'} + S_{I2}^{M(1)}\right] \\ -\left[\lambda_2^{'} + S_{12}^{M(1)}\right]\left[\lambda_2^{'} + S_{I1}^{M(1)}\right] \end{array}\right\}}{\left\{\begin{array}{c} 2\left[\lambda_2^{'} + \mu_2^{'} + S_{22}^{M(1)} + S_{22}^{M(2)}\right]\left[\lambda_2^{'} + 2\mu_2^{'} + S_{11}^{M(1)} + 2S_{11}^{M(2)}\right] \\ -2\left[\lambda_2^{'} + S_{12}^{M(1)}\right]\left[\lambda_2^{'} + S_{21}^{M(1)}\right] \end{array}\right\}} \tag{109}$$

$$\Psi_{I1}^{(3)} = \frac{\left[\lambda_3^{'} + \mu_3^{'} + S_{22}^{M(3)} + S_{22}^{M(4)}\right]\left[\lambda_3^{'} + S_{I1}^{M(3)}\right] - \left[\lambda_3^{'} + S_{21}^{M(3)}\right]\left[\lambda_3^{'} + S_{I2}^{M(3)}\right]}{\left\{\begin{array}{c}\left[\lambda_3^{'} + \mu_3^{'} + S_{22}^{M(3)} + S_{22}^{M(4)}\right]\left[\lambda_3^{'} + 2\mu_3^{'} + S_{11}^{M(3)} + 2S_{11}^{M(4)}\right] \\ -\left[\lambda_3^{'} + S_{12}^{M(3)}\right]\left[\lambda_3^{'} + S_{21}^{M(3)}\right]\end{array}\right\}} \tag{110}$$

$$\Psi_{I2}^{(3)} = \Psi_{I3}^{(3)} = \frac{\left\{\begin{array}{c}\left[\lambda_3^{'} + 2\mu_3^{'} + S_{11}^{M(3)} + 2S_{11}^{M(4)}\right]\left[\lambda_3^{'} + S_{I2}^{M(3)}\right] \\ -\left[\lambda_3^{'} + S_{12}^{M(3)}\right]\left[\lambda_3^{'} + S_{I1}^{M(3)}\right]\end{array}\right\}}{\left\{\begin{array}{c}2\left[\lambda_3^{'} + \mu_3^{'} + S_{22}^{M(3)} + S_{22}^{M(4)}\right]\left[\lambda_3^{'} + 2\mu_3^{'} + S_{11}^{M(3)} + 2S_{11}^{M(4)}\right] \\ -2\left[\lambda_3^{'} + S_{12}^{M(3)}\right]\left[\lambda_3^{'} + S_{21}^{M(3)}\right]\end{array}\right\}} \tag{111}$$

$$\Psi_{I1}^{(4)} = \frac{\left[S_{22}^{(1)} + S_{22}^{(2)} - 2 + 2\nu_0\right] S_{I1}^{(1)} - S_{21}^{(1)} S_{I2}^{(1)}}{\left[S_{22}^{(1)} + S_{22}^{(2)} - 2 + 2\nu_0\right]\left[S_{11}^{(1)} + 2S_{11}^{(2)} - 4 + 4\nu_0\right] - S_{12}^{(1)} S_{21}^{(1)}} \tag{112}$$

$$\Psi_{I2}^{(4)} = \Psi_{I3}^{(4)} = \frac{\left[S_{11}^{(1)} + 2S_{11}^{(2)} - 4 + 4\nu_0\right] S_{I2}^{(1)} - S_{12}^{(1)} S_{I1}^{(1)}}{2\left[S_{22}^{(1)} + S_{22}^{(2)} - 2 + 2\nu_0\right]\left[S_{11}^{(1)} + 2S_{11}^{(2)} - 4 + 4\nu_0\right] - 2S_{12}^{(1)} S_{21}^{(1)}} \tag{113}$$

and

$$\lambda_r^{'} = \frac{4(1-\nu_0)(\mu_r\lambda_0 - \mu_0\lambda_r)}{(\mu_r - \mu_0)\left[3(\lambda_r - \lambda_0) + 2(\mu_r - \mu_0)\right]}, \qquad \mu_r^{'} = \frac{2\mu_0(1-\nu_0)}{\mu_r - \mu_0} \tag{114}$$

Appendix C Parameters $\Upsilon_1, \ldots, \Upsilon_8$ and $\Theta_1, \ldots, \Theta_8$ in Eq. (39)

$$\Upsilon_1 = \frac{\left[S_{11}^{(1)} + 4S_{21}^{(1)} + 2S_{11}^{(2)}\right]\left[1 - \Psi_{11}^{(1)} - 4\Psi_{12}^{(1)}\right] + 10S_{21}^{(1)}\Psi_{12}^{(1)}}{30\left[\mu_1^{'} + S_{11}^{(2)}\right]} - \frac{2S_{12}^{(2)}}{15\left[\mu_1^{'} + S_{12}^{(2)}\right]} + \frac{\left[3S_{22}^{(1)} + 2S_{12}^{(1)} + 3S_{22}^{(2)}\right]\left[3 - 4\Psi_{21}^{(1)} - 6\Psi_{22}^{(1)}\right] - 6S_{22}^{(2)} + 5S_{12}^{(1)}\Psi_{21}^{(1)}}{45\left[\mu_1^{'} + S_{22}^{(2)}\right]} \tag{115}$$

$$\Upsilon_2 = \frac{\left[S_{11}^{(1)} - S_{21}^{(1)} + 2S_{11}^{(2)}\right]\left[1 - \Psi_{11}^{(1)} + \Psi_{12}^{(1)}\right]}{30\left[\mu_1^{'} + S_{11}^{(2)}\right]} + \frac{S_{12}^{(2)}}{5\left[\mu_1^{'} + S_{12}^{(2)}\right]} + \frac{\left[S_{22}^{(1)} - S_{12}^{(1)} + S_{22}^{(2)}\right]\left[1 + 2\Psi_{21}^{(1)} - 2\Psi_{22}^{(1)}\right] + 6S_{22}^{(2)}}{30\left[\mu_1^{'} + S_{22}^{(2)}\right]} \tag{116}$$

$$\Upsilon_3 = \frac{\left[S_{11}^{M(1)} + 4S_{21}^{M(1)} + 2S_{11}^{M(2)}\right]\left[1 - \Psi_{11}^{(2)} - 4\Psi_{12}^{(2)}\right] + 10S_{21}^{M(1)}\Psi_{12}^{(2)}}{30\left[\mu_2' + S_{11}^{M(2)}\right]}$$
$$- \frac{2S_{12}^{M(2)}}{15\left[\mu_2' + S_{12}^{M(2)}\right]}$$
$$+ \frac{\left[3S_{22}^{M(1)} + 2S_{12}^{M(1)} + 3S_{22}^{M(2)}\right]\left[3 - 4\Psi_{21}^{(2)} - 6\Psi_{22}^{(2)}\right] - 6S_{22}^{M(2)} + 5S_{12}^{M(1)}\Psi_{21}^{(2)}}{45\left[\mu_2' + S_{22}^{M(2)}\right]} \quad (117)$$

$$\Upsilon_4 = \frac{\left[S_{11}^{M(1)} - S_{21}^{M(1)} + 2S_{11}^{M(2)}\right]\left[1 - \Psi_{11}^{(2)} + \Psi_{12}^{(2)}\right]}{30\left[\mu_2' + S_{11}^{M(2)}\right]} + \frac{S_{12}^{M(2)}}{5\left[\mu_2' + S_{12}^{M(2)}\right]}$$
$$+ \frac{\left[S_{22}^{M(1)} - S_{12}^{M(1)} + S_{22}^{M(2)}\right]\left[1 + 2\Psi_{21}^{(2)} - 2\Psi_{22}^{(2)}\right] + 6S_{22}^{M(2)}}{30\left[\mu_2' + S_{22}^{M(2)}\right]} \quad (118)$$

$$\Upsilon_5 = \frac{\left[S_{11}^{M(3)} + 4S_{21}^{M(3)} + 2S_{11}^{M(4)}\right]\left[1 - \Psi_{11}^{(3)} - 4\Psi_{12}^{(3)}\right] + 10S_{21}^{M(3)}\Psi_{12}^{(3)}}{30\left[\mu_3' + S_{11}^{M(4)}\right]}$$
$$- \frac{2S_{12}^{M(4)}}{15\left[\mu_3' + S_{12}^{M(4)}\right]}$$
$$+ \frac{\left[3S_{22}^{M(3)} + 2S_{12}^{M(3)} + 3S_{22}^{M(4)}\right]\left[3 - 4\Psi_{21}^{(3)} - 6\Psi_{22}^{(3)}\right] - 6S_{22}^{M(4)} + 5S_{12}^{M(3)}\Psi_{21}^{(3)}}{45\left[\mu_3' + S_{22}^{M(4)}\right]} \quad (119)$$

$$\Upsilon_6 = \frac{\left[S_{11}^{M(3)} - S_{21}^{M(3)} + 2S_{11}^{M(4)}\right]\left[1 - \Psi_{11}^{(3)} + \Psi_{12}^{(3)}\right]}{30\left[\mu_3' + S_{11}^{M(4)}\right]} + \frac{S_{12}^{M(4)}}{5\left[\mu_3' + S_{12}^{M(4)}\right]}$$
$$+ \frac{\left[S_{22}^{M(3)} - S_{12}^{M(3)} + S_{22}^{M(4)}\right]\left[1 + 2\Psi_{21}^{(3)} - 2\Psi_{22}^{(3)}\right] + 6S_{22}^{M(4)}}{30\left[\mu_3' + S_{22}^{M(4)}\right]} \quad (120)$$

$$\Upsilon_7 = \frac{\left[S_{11}^{(1)} + 4S_{21}^{(1)} + 2S_{11}^{(2)}\right]\left[1 - \Psi_{11}^{(4)} - 4\Psi_{12}^{(4)}\right] + 10S_{21}^{(1)}\Psi_{12}^{(4)}}{30\left[-2 + 2\nu_0 + S_{11}^{(2)}\right]} - \frac{2S_{12}^{(2)}}{15\left[-2 + 2\nu_0 + S_{12}^{(2)}\right]} + \frac{\left[3S_{22}^{(1)} + 2S_{12}^{(1)} + 3S_{22}^{(2)}\right]\left[3 - 4\Psi_{21}^{(4)} - 6\Psi_{22}^{(4)}\right] - 6S_{22}^{(2)} + 5S_{12}^{(1)}\Psi_{21}^{(4)}}{45\left[-2 + 2\nu_0 + S_{22}^{(2)}\right]} \quad (121)$$

$$\Upsilon_8 = \frac{\left[S_{11}^{(1)} - S_{21}^{(1)} + 2S_{11}^{(2)}\right]\left[1 - \Psi_{11}^{(4)} + \Psi_{12}^{(4)}\right]}{30\left[-2 + 2\nu_0 + S_{11}^{(2)}\right]} + \frac{S_{12}^{(2)}}{5\left[-2 + 2\nu_0 + S_{12}^{(2)}\right]} + \frac{\left[S_{22}^{(1)} - S_{12}^{(1)} + S_{22}^{(2)}\right]\left[1 + 2\Psi_{21}^{(4)} - 2\Psi_{22}^{(4)}\right] + 6S_{22}^{(2)}}{30\left[-2 + 2\nu_0 + S_{22}^{(2)}\right]} \quad (122)$$

$$\Theta_1 = \frac{2(1-\nu_0)}{15}\left[\frac{1 - \Psi_{11}^{(1)} - 4\Psi_{12}^{(1)}}{\mu_1' + S_{11}^{(2)}} - \frac{2}{\mu_1' + S_{12}^{(2)}} + \frac{1 - 4\Psi_{21}^{(1)} - 6\Psi_{22}^{(1)}}{\mu_1' + S_{22}^{(2)}}\right] \quad (123)$$

$$\Theta_2 = \frac{1-\nu_0}{15}\left[\frac{2 - 2\Psi_{11}^{(1)} + 2\Psi_{12}^{(1)}}{\mu_1' + S_{11}^{(2)}} + \frac{6}{\mu_1' + S_{12}^{(2)}} + \frac{7 + 2\Psi_{21}^{(1)} - 2\Psi_{22}^{(1)}}{\mu_1' + S_{22}^{(2)}}\right] \quad (124)$$

$$\Theta_3 = \frac{2(1-\nu_0)}{15}\left[\frac{1 - \Psi_{11}^{(2)} - 4\Psi_{12}^{(2)}}{\mu_2' + S_{11}^{M(2)}} - \frac{2}{\mu_2' + S_{12}^{M(2)}} + \frac{1 - 4\Psi_{21}^{(2)} - 6\Psi_{22}^{(2)}}{\mu_2' + S_{22}^{M(2)}}\right] \quad (125)$$

$$\Theta_4 = \frac{1-\nu_0}{15}\left[\frac{2 - 2\Psi_{11}^{(2)} + 2\Psi_{12}^{(2)}}{\mu_2' + S_{11}^{M(2)}} + \frac{6}{\mu_2' + S_{12}^{M(2)}} + \frac{7 + 2\Psi_{21}^{(2)} - 2\Psi_{22}^{(2)}}{\mu_2' + S_{22}^{M(2)}}\right] \quad (126)$$

$$\Theta_5 = \frac{2(1-\nu_0)}{15}\left[\frac{1 - \Psi_{11}^{(3)} - 4\Psi_{12}^{(3)}}{\mu_3' + S_{11}^{M(4)}} - \frac{2}{\mu_3' + S_{12}^{M(4)}} + \frac{1 - 4\Psi_{21}^{(3)} - 6\Psi_{22}^{(3)}}{\mu_3' + S_{22}^{M(4)}}\right] \quad (127)$$

$$\Theta_6 = \frac{1-\nu_0}{15}\left[\frac{2 - 2\Psi_{11}^{(3)} + 2\Psi_{12}^{(3)}}{\mu_3' + S_{11}^{M(4)}} + \frac{6}{\mu_3' + S_{12}^{M(4)}} + \frac{7 + 2\Psi_{21}^{(3)} - 2\Psi_{22}^{(3)}}{\mu_3' + S_{22}^{M(4)}}\right] \quad (128)$$

$$\Theta_7 = \frac{2(1-\nu_0)}{15}\left[\frac{1 - \Psi_{11}^{(4)} - 4\Psi_{12}^{(4)}}{-2 + 2\nu_0 + S_{11}^{(2)}} - \frac{2}{-2 + 2\nu_0 + S_{12}^{(2)}} + \frac{1 - 4\Psi_{21}^{(4)} - 6\Psi_{22}^{(4)}}{-2 + 2\nu_0 + S_{22}^{(2)}}\right] \quad (129)$$

$$\Theta_8 = \frac{1-\nu_0}{15}\left[\frac{2 - 2\Psi_{11}^{(4)} + 2\Psi_{12}^{(4)}}{-2 + 2\nu_0 + S_{11}^{(2)}} + \frac{6}{-2 + 2\nu_0 + S_{12}^{(2)}} + \frac{7 + 2\Psi_{21}^{(4)} - 2\Psi_{22}^{(4)}}{-2 + 2\nu_0 + S_{22}^{(2)}}\right] \quad (130)$$

Appendix D Parameters $\hat{\Psi}_{IJ}^{(1)},\ldots,\hat{\Psi}_{IJ}^{(4)}$ in Eqs. (45) – (58)

$$\hat{\Psi}_{I1}^{(1)}=\frac{\left[2-2\nu_0+\hat{\xi}_{22}^{(1)}+2\hat{\mu}_1 S_{22}^{(2)}\right]\hat{\xi}_{I1}^{(1)}-\hat{\xi}_{21}^{(1)}\hat{\xi}_{I2}^{(1)}}{\left[2-2\nu_0+\hat{\xi}_{22}^{(1)}+2\hat{\mu}_1 S_{22}^{(2)}\right]\left[4-4\nu_0+\hat{\xi}_{11}^{(1)}+4\hat{\mu}_1 S_{11}^{(2)}\right]-\hat{\xi}_{12}^{(1)}\hat{\xi}_{21}^{(1)}} \tag{131}$$

$$\hat{\Psi}_{I2}^{(1)}=\hat{\Psi}_{I3}^{(1)}=\frac{\left[4-4\nu_0+\hat{\xi}_{11}^{(1)}+4\hat{\mu}_1 S_{11}^{(2)}\right]\hat{\xi}_{I2}^{(1)}-\hat{\xi}_{12}^{(1)}\hat{\xi}_{I1}^{(1)}}{2\left[2-2\nu_0+\hat{\xi}_{22}^{(1)}+2\hat{\mu}_1 S_{22}^{(2)}\right]\left[4-4\nu_0+\hat{\xi}_{11}^{(1)}+4\hat{\mu}_1 S_{11}^{(2)}\right]-2\hat{\xi}_{12}^{(1)}\hat{\xi}_{21}^{(1)}} \tag{132}$$

$$\hat{\Psi}_{I1}^{(2)}=\frac{\left[2-2\nu_0+\hat{\xi}_{22}^{(2)}+2\hat{\mu}_2 S_{22}^{M(2)}\right]\hat{\xi}_{I1}^{(2)}-\hat{\xi}_{21}^{(2)}\hat{\xi}_{I2}^{(2)}}{\left[2-2\nu_0+\hat{\xi}_{22}^{(2)}+2\hat{\mu}_2 S_{22}^{M(2)}\right]\left[4-4\nu_0+\hat{\xi}_{11}^{(2)}+4\hat{\mu}_2 S_{11}^{M(2)}\right]-\hat{\xi}_{12}^{(2)}\hat{\xi}_{21}^{(2)}} \tag{133}$$

$$\hat{\Psi}_{I2}^{(2)}=\hat{\Psi}_{I3}^{(2)}=\frac{\left[4-4\nu_0+\hat{\xi}_{11}^{(2)}+4\hat{\mu}_2 S_{11}^{M(2)}\right]\hat{\xi}_{I2}^{(2)}-\hat{\xi}_{12}^{(2)}\hat{\xi}_{I1}^{(2)}}{\left\{\begin{array}{c}2\left[2-2\nu_0+\hat{\xi}_{22}^{(2)}+2\hat{\mu}_2 S_{22}^{M(2)}\right]\left[4-4\nu_0+\hat{\xi}_{11}^{(2)}+4\hat{\mu}_2 S_{11}^{M(2)}\right]\\ -2\hat{\xi}_{12}^{(2)}\hat{\xi}_{21}^{(2)}\end{array}\right\}} \tag{134}$$

$$\hat{\Psi}_{I1}^{(3)}=\frac{\left[2-2\nu_0+\hat{\xi}_{22}^{(3)}+2\hat{\mu}_3 S_{22}^{M(4)}\right]\hat{\xi}_{I1}^{(3)}-\hat{\xi}_{21}^{(3)}\hat{\xi}_{I2}^{(3)}}{\left[2-2\nu_0+\hat{\xi}_{22}^{(3)}+2\hat{\mu}_3 S_{22}^{M(4)}\right]\left[4-4\nu_0+\hat{\xi}_{11}^{(3)}+4\hat{\mu}_3 S_{11}^{M(4)}\right]-\hat{\xi}_{12}^{(3)}\hat{\xi}_{21}^{(3)}} \tag{135}$$

$$\hat{\Psi}_{I2}^{(3)}=\hat{\Psi}_{I3}^{(3)}=\frac{\left[4-4\nu_0+\hat{\xi}_{11}^{(3)}+4\hat{\mu}_3 S_{11}^{M(4)}\right]\hat{\xi}_{I2}^{(3)}-\hat{\xi}_{12}^{(3)}\hat{\xi}_{I1}^{(3)}}{\left\{\begin{array}{c}2\left[2-2\nu_0+\hat{\xi}_{22}^{(3)}+2\hat{\mu}_3 S_{22}^{M(4)}\right]\left[4-4\nu_0+\hat{\xi}_{11}^{(3)}+4\hat{\mu}_3 S_{11}^{M(4)}\right]\\ -2\hat{\xi}_{12}^{(3)}\hat{\xi}_{21}^{(3)}\end{array}\right\}} \tag{136}$$

$$\hat{\Psi}_{I1}^{(4)}=\frac{\left[2-2\nu_0-S_{22}^{(1)}-S_{22}^{(2)}\right]S_{I1}^{(1)}+S_{21}^{(1)}S_{I2}^{(1)}}{\left[2-2\nu_0-S_{22}^{(1)}-S_{22}^{(2)}\right]\left[4-4\nu_0-S_{11}^{(1)}-2S_{11}^{(2)}\right]-S_{12}^{(1)}S_{21}^{(1)}} \tag{137}$$

$$\hat{\Psi}_{I2}^{(4)}=\hat{\Psi}_{I3}^{(4)}=\frac{\left[4-4\nu_0-S_{11}^{(1)}-2S_{11}^{(2)}\right]S_{I2}^{(1)}+S_{12}^{(1)}S_{I1}^{(1)}}{2\left[2-2\nu_0-S_{22}^{(1)}-S_{22}^{(2)}\right]\left[4-4\nu_0-S_{11}^{(1)}-2S_{11}^{(2)}\right]-2S_{12}^{(1)}S_{21}^{(1)}} \tag{138}$$

where

$$\hat{\xi}_{IK}^{(1)}=2\hat{\mu}_1 S_{IK}^{(1)}+2\hat{\lambda}_1 S_{II}^{(2)}+\hat{\lambda}_1\sum_{n=1}^{3}S_{In}^{(1)} \tag{139}$$

$$\hat{\xi}_{IK}^{(2)} = 2\hat{\mu}_2 S_{IK}^{M(1)} + 2\hat{\lambda}_2 S_{II}^{M(2)} + \hat{\lambda}_2 \sum_{n=1}^{3} S_{In}^{M(1)} \tag{140}$$

$$\hat{\xi}_{IK}^{(3)} = 2\hat{\mu}_3 S_{IK}^{M(3)} + 2\hat{\lambda}_3 S_{II}^{M(4)} + \hat{\lambda}_3 \sum_{n=1}^{3} S_{In}^{M(3)} \tag{141}$$

with

$$\hat{\lambda}_r = \frac{\lambda_r \mu_0 - \lambda_0 \mu_r}{\mu_0(3\lambda_0 + 2\mu_0)}, \qquad \hat{\mu}_r = \frac{\mu_r - \mu_0}{2\mu_0} \tag{142}$$